CONTROL OF AN UNDERACTUATED SYSTEM AROUND A PERIODIC
ORBIT

A THESIS SUBMITTED TO
THE GRADUATE SCHOOL OF NATURAL AND APPLIED SCIENCES
OF
MIDDLE EAST TECHNICAL UNIVERSITY

BY

AYŞE DENİZ DUYUL

IN PARTIAL FULFILLMENT OF THE REQUIREMENTS
FOR
THE DEGREE OF MASTER OF SCIENCE
IN
ELECTRICAL AND ELECTRONICS ENGINEERING

SEPTEMBER 2018

Approval of the thesis:

CONTROL OF AN UNDERACTUATED SYSTEM AROUND A PERIODIC ORBIT

submitted by **AYŞE DENİZ DUYUL** in partial fulfillment of the requirements for the degree of **Master of Science in Electrical and Electronics Engineering Department, Middle East Technical University** by,

Prof. Dr. Halil Kalıpçılar
Dean, Graduate School of **Natural and Applied Sciences** ⸻

Prof. Dr. Tolga Çiloğlu
Head of Department, **Electrical and Electronics Engineering** ⸻

Assoc. Prof. Dr. Afşar Saranlı
Supervisor, **Electrical and Electronics Eng., METU** ⸻

Assist. Prof. Dr. Mustafa Mert Ankaralı
Co-supervisor, **Electrical and Electronics Eng., METU** ⸻

Examining Committee Members:

Prof. Dr. Kemal Leblebicioğlu
Electrical and Electronics Eng. Dep., METU ⸻

Assoc. Prof. Dr. Afşar Saranlı
Electrical and Electronics Eng. Dep., METU ⸻

Assist. Prof. Dr. Mustafa Mert Ankaralı
Electrical and Electronics Eng. Dep., METU ⸻

Prof. Dr. Ömer Morgül
Electrical Eng. Dep., Bilkent University ⸻

Assist. Prof. Dr. Emre Özkan
Electrical and Electronics Eng. Dep., METU ⸻

Date: __04.09.2018__

I hereby declare that all information in this document has been obtained and presented in accordance with academic rules and ethical conduct. I also declare that, as required by these rules and conduct, I have fully cited and referenced all material and results that are not original to this work.

Name, Last Name: AYŞE DENİZ DUYUL

Signature   :

ABSTRACT

CONTROL OF AN UNDERACTUATED SYSTEM AROUND A PERIODIC ORBIT

Duyul, Ayşe Deniz

M.S., Department of Electrical and Electronics Engineering

Supervisor   : Assoc. Prof. Dr. Afşar Saranlı

Co-Supervisor   : Assist. Prof. Dr. Mustafa Mert Ankaralı

September 2018, 62 pages

Quasi-periodic behavior is one of the most important fundamental building blocks for locomotion in biological (and robotic) systems. The dynamics that govern the motion of such behaviors are generally highly nonlinear and underactuated. One method of analyzing the quasi-periodic behaviors of such systems is to linearize the system around these periodic trajectories. Such a linearization provides us a linear time periodic (LTP) system around the neighborhood of the periodic orbit. Analysis and control of LTP systems has gained some attention in the last decade and various methods have emerged for this purpose. One of these methods, which we focus on this thesis, is the harmonic balance approach. In the literature harmonic balance and harmonic transfer functions based approaches have been mostly utilized in system identification. There are very few methods that adopt these approaches for control and stabilization purposes. In this thesis, we propose a control method which can generate stable periodic behaviors for underactuated nonlinear robotic systems. We first generate a reference periodic orbit that can be tracked by the given system and

find the open-loop control input that can achieve this trajectory. We then linearize the equations of motion to obtain an LTP representation around the given periodic orbit. Finally, we propose a linear time invariant state feedback control law based on eigenvalue optimization of the lifted LTI representation of the LTP system (harmonic balance). We applied our method on the widely used cart-pendulum example in simulation environment for limit cycles around both stable and unstable equilibrium points. We obtained succesful results for limit cycles around the stable equilibrium point enhancing system performance and tracking position, amlitude and phase changes in the limit cycle. For limit cycles around the unstable equilibrium point, we obtained stable periodic orbits and promising directions for future studies.

ÖZ

EKSİK TAHRİKLİ BİR SİSTEMİN PERİYODİK YÖRÜNGE ÇEVRESİNDE KONTROLÜ

Duyul, Ayşe Deniz

Yüksek Lisans, Elektrik ve Elektronik Mühendisliği Bölümü

Tez Yöneticisi   : Doç. Dr. Afşar Saranlı

Ortak Tez Yöneticisi   : Dr. Öğr. Üyesi Mustafa Mert Ankaralı

Eylül 2018 , 62 sayfa

Yarı periyodik davranış biyolojik ve robotik sistemlerde hareketin en önemli yapı unsurlarından biridir. Bu tarz davranışları tarif eden dinamikler genellikle yüksek derecede doğrusal değil ve eksik tahriklidir. Böyle sistemlerdeki yarı periyodik davranışı incelemenin bir yöntemi de bu sistemleri periyodik yörüngeler etrafında doğrusallaştırmaktır. Bu doğrusallaştırma sonucu periyodik yörüngenin yakınında geçerli doğrusal zamanla periyodik değişen (DZPD) bir sistem elde ederiz. DZPD sistemlerin incelenmesi ve kontrolü son on yılda ilgi kazanmış olup çeşitli yöntemler ortaya çıkmıştır. Bu yöntemlerin bir tanesi de, bu tezde de odaklandığımız harmonik denge yaklaşımıdır. Literatürde harmonik denge ve harmonik transfer fonksiyonları çoğunlukla sistem tanılaması amacıyla kullanılmakta olup kontrol amacıyla bu yaklaşımları kullanan çok az yöntem vardır. Bu tezde, eksik tahrikli doğrusal olmayan robotik sistemlerde kararlı periyodik davranışlar oluşturabilecek bir kontrol yöntemi öne sürüyoruz. Öncelikle, elimizdeki sistem tarafından takip edilebilecek bir referans yörüngesi oluş-

turup bu yörüngeyi sağlayacak açık döngü kontrolcüsünü elde ediyoruz. Daha sonra, hareket denklemlerini bu periyodik yörünge etrafında doğrusallaştırarak doğrusal olmayan sistemin DZPD yakınsamasını elde ediyoruz. Son olarak da, elde edilen DZPD sistemin harmonik denge yöntemi ile elde edilmiş doğrusal zamanla değişmez (DZD) temsili üzerinden özdeğer optimizasyonuna dayanan DZD bir durum geri beslemesi kontrol kuralı öne sürüyoruz. Bu yöntemi literatürde çokça kullanılan araba-sarkaç modeli üzerinde simulasyon ortamında kararlı ve kararsız denge noktaları etrafında tanımlanmış periyodik yörüngelere uyguladık. Kararlı denge noktası etrafındaki periyodik yörüngeler için, sistem performansını geliştiren ve periyodik yörüngedeki konum, genlik ve faz değişikliklerini takip edebilen başarılı sonuçlar elde ettik. Kararsız denge noktası etrafındaki periyodik yörüngeler içinse, kararlı periyodik yörüngeler ve gelecek çalışmalar için umut vaadeden sonuçlar elde ettik.

Anahtar Kelimeler: Eksik-Tahrikli Sistemler, Doğrusal Zamanla Periyodik Değişen Sistemler, Harmonik Denge

To my father

ACKNOWLEDGMENTS

TABLE OF CONTENTS

LIST OF TABLES

LIST OF FIGURES

FIGURES

LIST OF ABBREVIATIONS

LTI	Linear Time Invariant
LTV	Linear Time Varying
LTP	Linear Time Periodic
HTF	Harmonic Transfer Function
EMP	Exponentially Modulated Periodic

CHAPTER 1

INTRODUCTION

Periodic motion is a significant component for many robotic and biological applications, especially for legged locomotion [1–7]. Generation and stabilization of periodic trajectories in these systems is a challenging task since the dynamics describing such systems are generally highly nonlinear and underactuated. Linearization is a potentially powerful tool for addressing this challenge due to the well developed linear systems theory. In many cases, nonlinear systems operating around a periodic orbit are approximated with linear time periodic (LTP) systems using a linearization tool such as trajectory linearization, transverse linearization or feedback linearization. In addition to locomotion examples [8–10], there are many application domains in the literature such as wind turbines [11, 12], helicopter rotors [13, 14] and power systems [15–18] that are also modeled as LTP systems. Some methods developed for LTI systems can be extended to hold for LTP systems as well due to the periodicity of the time varying aspect. However, analysis and control of LTP systems is much more challenging than the LTI cases.

One of most frequent methods used for planning periodic trajectories in underactuated nonlinear systems is the virtual holonomic constraints [1, 19–25]. In [23, 25] the system is linearized around a periodic trajectory via transverse linearization, resulting in an LTP system and they apply stabilizing controllers using the time varying linear quadratic regulator (LQR) solution. On the other hand, some other studies [19, 24] utilize partial feedback linearization to obtain the LTP structure, which is again stabilized by an LQR-based control law. Ames et al. [1] adopts control Lyapunov functions in order to exponentially stabilize periodic trajectories. Various different methods

1

without LTP system approximation also exist in the literature [2, 26].

One of the most fundamental tools for the analysis of LTP systems were developed by Floquet in 1883 [27]. Floquet theory introduces a time periodic similarity transformation, which transforms the time periodic dynamic matrix into a time invariant one. This basically allows the application of stability and some other analysis methods developed for LTI systems, to LTP systems. Lyapunov functions [28–30] and Hill determinant method [31] are also available for stability analysis of LTP systems. Another important tool for analysis of LTP systems is the concept of Harmonic Transfer Functions (HTF) [32] which are similar to the transfer functions of LTI systems, modeling the linear relationship between harmonics of the input and output of LTP systems. HTF's allow the adaptation of Nyquist stability criterion to LTP systems [32–34], which is similar to the generalized Nyquist criterion for multi-input multi-output LTI systems. Nyquist criterion is advantageous to previously mentioned techniques since it can give closed-loop stability information for a range of feedback gains.

For control of LTP systems, most popularly used method is LQR, which provides an "optimal" time periodic state feedback gain guaranteeing stability of the closed-loop system [13, 35]. Static-feedback gain controllers based on Nyquist criterion are also studied in the literature [32, 34]. Frequency domain representation based analysis of LTP systems have gained substantial attraction recently in system identification literature [8, 36–39]. Yet, very few control methodologies exist that utilize frequency domain based formulations. We propose a control method based on the harmonic balance concept [31] which can generate stable oscillations of underactuated nonlinear robotic systems. We start under the assumption of existence of periodic orbits that are trackable by the system and proceed to determine the open-loop control input that will force the dynamics to exhibit the assumed periodic behavior. Then, we linearize the equations of motion around this periodic trajectory to obtain an LTP approximation representing the system dynamics in the vicinity of the periodic orbit. Finally, we obtain the truncated lifted LTI representation of the LTP approximation and by optimization of the eigenvalues of this LTI form we obtain a static gain state feedback control law enhancing the system performance for stable limit cycles. We also investigate the performance of our method for unstable limit cycles. Through a more

intricate optimization procedure we achieve stable behavior and draw conclusions for possible enhancements. We applied our method on the widely used cart-pendulum example obtaining oscillations around the vertical.

Organization of this thesis is as follows. In Chapter 2, we provide some mathematical background information related to our work. We first address the concept of trajectory linearization, and then we examine three different analysis methods for LTP systems. We go over time-domain analysis of LTP systems, Floquet theory, and frequency domain analysis of LTP systems in state space form with emphasis on harmonic balance. In Chapter 3, we introduce an LTI state feedback control methodology for orbital stabilization of nonlinear underactuated systems based on linearization around a periodic orbit and harmonic balance representation of the LTP system around this periodic orbit. In Chapter 4, we present simulation results of the developed control method around stable and unstable limit cycles of the cart-pendulum system example. In Chapter 5, we provide conclusions on the performance and limitations of the developed method and discuss some possible future work.

CHAPTER 2

MATHEMATICAL BACKGROUND

In this chapter, we will go over some relevant mathematical background information. First, we will remember the concept of linearization and how it is applied around a trajectory. Second, we will explain basic analysis methods used for LTP systems.

2.1 Trajectory Linearization

Linearization is the most fundamental approach in order to locally (around an equilibrium point or a trajectory) analyze and control nonlinear systems. The obvious advantage is that one can make use of the well developed linear systems theory tools around the approximately linear region. A nonlinear system,

$$\frac{dx(t)}{dt} = f(x(t), u(t))$$
$$y(t) = h(x(t), u(t))$$

(2.1)

where $x \in \Re^n$, $u \in \Re^m$, and $y \in \Re^p$ are the state, input and output vectors respectively, is linearized around its equilibrium points resulting in a linear time invariant (LTI) system describing the local behavior in the neighborhood of the linearization point,

$$\frac{dx(t)}{dt} = Ax(t) + Bu(t))$$
$$y(t) = Cx(t) + Du(t)$$

(2.2)

5

where $A \in \Re^{nxn}$, $B \in \Re^{nxm}$, $C \in \Re^{pxn}$, and $D \in \Re^{mxp}$ are constant matrices.

If the goal is not to stabilize the system at an equilibrium point but to track a trajectory, linearization can also be utilized to describe the reaction of the system to small deviations from a given trajectory resulting in a linear time varying (LTV) system.

Linearization around a trajectory is performed in the same way as linearization around an equilibrium point using a Taylor expansion. Let $\{x_0(t), u_0(t)\}$ be a solution to the system of equations (2.1).

$$\frac{dx_0(t)}{dt} = f(x_0(t), u_0(t))$$
$$y_0(t) = h(x_0(t), u_0(t)) \tag{2.3}$$

Neglecting the higher order terms, Taylor expansion around this solution will be

$$\frac{dx(t)}{dt} = f(x_0(t), u_0(t)) + \frac{\partial f(x(t), u(t))}{\partial x(t)}\bigg|_{\substack{x(t)=x_0(t) \\ u(t)=u_0(t)}} (x(t) - x_0(t))$$
$$+ \frac{\partial f(x(t), u(t))}{\partial u(t)}\bigg|_{\substack{x(t)=x_0(t) \\ u(t)=u_0(t)}} (u(t) - u_0(t))$$
$$y(t) = h(x_0(t), u_0(t)) + \frac{\partial h(x(t), u(t))}{\partial x(t)}\bigg|_{\substack{x(t)=x_0(t) \\ u(t)=u_0(t)}} (x(t) - x_0(t)) \tag{2.4}$$
$$+ \frac{\partial h(x(t), u(t))}{\partial u(t)}\bigg|_{\substack{x(t)=x_0(t) \\ u(t)=u_0(t)}} (u(t) - u_0(t))$$

where $x(t) = x_0(t) + \bar{x}(t)$, $u(t) = u_0(t) + \bar{u}(t)$, and $y(t) = y_0(t) + \bar{y}(t)$.

After making the necessary substitutions and rearrangements in equation (2.4) we obtain an LTV system

$$\frac{d\bar{x}(t)}{dt} = A(t)\bar{x}(t) + B(t)\bar{u}(t))$$
$$\bar{y}(t) = C(t)\bar{x}(t) + D(t)\bar{u}(t) \tag{2.5}$$

with

$$A(t) = \left.\frac{\partial f(x(t), u(t))}{\partial x(t)}\right|_{\substack{x(t)=x_0(t) \\ u(t)=u_0(t)}}, \quad B(t) = \left.\frac{\partial f(x(t), u(t))}{\partial u(t)}\right|_{\substack{x(t)=x_0(t) \\ u(t)=u_0(t)}},$$

$$\tag{2.6}$$

$$C(t) = \left.\frac{\partial h(x(t), u(t))}{\partial x(t)}\right|_{\substack{x(t)=x_0(t) \\ u(t)=u_0(t)}}, \quad D(t) = \left.\frac{\partial h(x(t), u(t))}{\partial u(t)}\right|_{\substack{x(t)=x_0(t) \\ u(t)=u_0(t)}},$$

If the trajectory $\{x_0(t), u_0(t)\}$ is periodic, system of equations (2.5) will be a linear time periodic (LTP) system where the system matrices $A(t)$, $B(t)$, $C(t)$, and $D(t)$, are all periodic with the same period.

2.2 Linear Time Periodic Systems

Many of the simple methods developed for LTI systems do not apply to a general LTV system. On the other hand, due to the periodicity some of these methods can be extended to hold for LTP systems.

2.2.1 Time Domain Analysis

For a general LTV system

$$\frac{dx(t)}{dt} = A(t)x(t) + B(t)u(t))$$

$$y(t) = C(t)x(t) + D(t)u(t) \tag{2.7}$$

the time domain solution is given by

$$x(t) = \Phi(t, t_0)x_0 + \int_{t_0}^{t} \Phi(t, \tau)B(\tau)u(\tau)d\tau \tag{2.8}$$

where $\Phi(t, t_0)$ is the state transition matrix satisfying the relationship

$$\frac{\partial \Phi(t, \tau)}{\partial t} = A(t)\Phi(t, \tau) \tag{2.9}$$

Ordinarily, neither $A(t)$ nor $\Phi(t, t_0)$ gives any stability information similar to an LTI case for time varying systems. However, for LTP systems where the system matrices $A(t)$, $B(t)$, $C(t)$, and $D(t)$, are all periodic with *pumping period* T, there is a special

7

case of state transition matrix giving (necessary and sufficient) stability information. State transition matrix over one period,

$$\Phi(T, 0) = \Phi(t + T, t) \tag{2.10}$$

is called the *monodromy matrix* of the system, and its eigenvalues are independent of t. An LTP system (2.7) is asymptotically stable if and only if all the eigenvalues of the monodromy matrix, also called the characteristic multipliers of $\mathcal{A}(t)$ are inside the open unit disk. On the other hand, it is very difficult if not impossible to obtain the state transition matrix analytically for general LTP systems. Usually, numerical integration methods are used to extract these kind of information which has some obvious limitations.

2.2.2 Floquet Decomposition

Floquet in 1883 [27] developed one of the most fundemental theorems for LTP systems. It states that for an LTP system in state space form (2.7), the state transition matrix (if nonsingular) can be expressed as,

$$\Phi(t, \tau) = P(t) e^{\bar{A}(t - \tau)} P^{-1}(\tau) \tag{2.11}$$

where $P(t)$ is a nonsingular, T-periodic matrix used in the state transformation $x(t) = P(t)z(t)$ and $\bar{A}$ is a constant, possibly complex system matrix of the newly defined dynamics,

$$\frac{dz(t)}{dt} = \bar{A}z(t) + \bar{B}(t)u(t))$$
$$\bar{y}(t) = \bar{C}(t)z(t) + D(t)u(t) \tag{2.12}$$

where,

$$\bar{A} = P^{-1}(t)(A(t)P(t) - \dot{P}(t)),$$
$$\bar{B}(t) = P^{-1}B(t), \tag{2.13}$$
$$\bar{C}(t) = C(t)P(t)$$

It can be deduced from equation (2.11), if $P(0) = P(T) = I$

$$e^{\bar{A}T} = \Phi(T, 0) \tag{2.14}$$

8

Equation (2.14) implies that if the eigenvalues of $\bar{A}$ are strictly negative than the eigenvalues of the monodromy matrix will stay strictly inside the open unit disk which is the necessary and sufficient condition for the stability of LTP systems as can be recalled from Section 2.2.1.

Using Floquet theorem, we can fully represent an LTP system having a time periodic system matrix $A(t)$, with another LTP system having a time invariant system matrix $\bar{A}$ and investigate the stability of the open-loop time periodic system with time invariant methods. However, if we introduce feedback into the loop, time periodic dynamics of the system become effective again and Floquet decomposition needs to be re-evaluated to analyze the stability of the closed loop system.

2.2.3 Frequency Response of LTP Systems

If a complex exponential signal

$$u(t) = u_0 e^{j\omega t}, \; u_0 \in \mathbb{C}^m \tag{2.15}$$

is fed to an LTI system (2.2) as the input the state and output vectors in steady state will also be complex exponents of the same frequency with probably different amplitudes.

$$\begin{aligned} x(t) &= x_0 e^{j\omega t}, \; x_0 \in \mathbb{C}^n \\ y(t) &= y_0 e^{j\omega t}, \; y_0 \in \mathbb{C}^p \end{aligned} \tag{2.16}$$

This, frequency separation property, leads to the definition of transfer function concept which greatly simplifies the analysis of LTI systems in frequency domain. However, LTP systems do not respond to sinusoids in the same way as LTI systems. If an LTP system is excited with a sinusoidal signal, the output signal will be comprised of many frequencies that are modulations of the input frequency with harmonics of the pumping frequency ω_0 (the fundamental frequency of the LTP system matrices) as

$$\omega_{out} = \omega + n\omega_0, \; n \in \mathbb{Z} \tag{2.17}$$

The input frequency is existent in the output only if there is a DC component of the **system dynamics**. Unless the input frequency is an integer multiple of the pumping frequency or the input frequency $\omega = 0$, pumping frequency is not directly observed in the output signal.

9

To better explain the frequency separation issue consider the following LTI and LTP systems:

$$\text{LTI} : \dot{x} = \begin{bmatrix} 0 & 1 \\ -1 & -1 \end{bmatrix} x + \begin{bmatrix} 0 \\ 1 \end{bmatrix} u$$
$$y = \begin{bmatrix} 1 & 0 \end{bmatrix} x \tag{2.18}$$

$$\text{LTP} : \dot{x} = \begin{bmatrix} 0 & 1 \\ -1 + cos(2\omega_0 t) & -1 + 3cos(\omega_0 t) \end{bmatrix} x + \begin{bmatrix} 0 \\ 1 \end{bmatrix} u$$
$$y = \begin{bmatrix} 1 & 0 \end{bmatrix} x \tag{2.19}$$

where $\omega_0 = 5 \ rad/sec$. When excited with a sinusoidal input $u = sin(\omega t)$ these systems produce outputs with frequency components as illustrated in Figure 2.1.

Wereley et al. [32] defined exponentially modulated periodic (EMP) signal concept as a *fundamental signal space*, in order to introduce a frequency response concept for LTP systems. When an EMP signal,

$$u(t) = \sum_n u_n e^{s_n t}, \ s_n = s + j\omega_0 n, \ n \in \mathbb{Z}, s \in \mathbb{C} \tag{2.20}$$

is supplied to an LTP system as an input, it leads to a state vector and an output of the same form in steady state.

$$x(t) = \sum_n x_n e^{s_n t}$$
$$\dot{x}(t) = \sum_n s_n x_n e^{s_n t} \tag{2.21}$$
$$y(t) = \sum_n y_n e^{s_n t}$$

Since the state-space system matrices are all periodic, they can be expressed as a complex Fourier series,

$$A(t) = \sum_n A_n e^{jn\omega_0 t}$$
$$B(t) = \sum_n B_n e^{jn\omega_0 t}$$
$$C(t) = \sum_n C_n e^{jn\omega_0 t} \tag{2.22}$$
$$D(t) = \sum_n D_n e^{jn\omega_0 t}$$
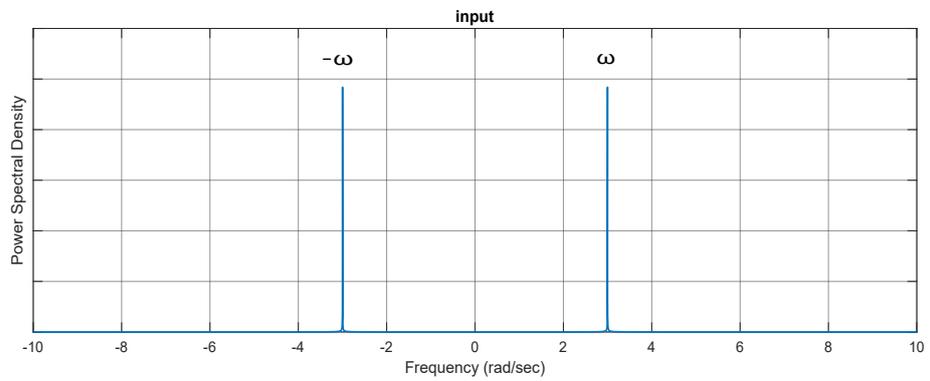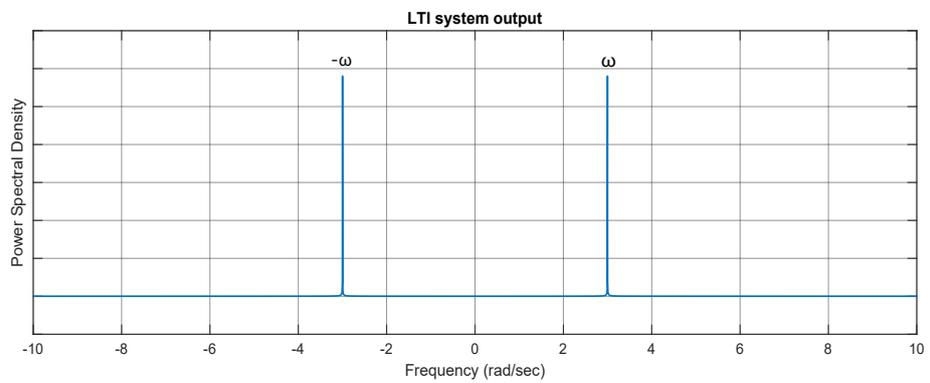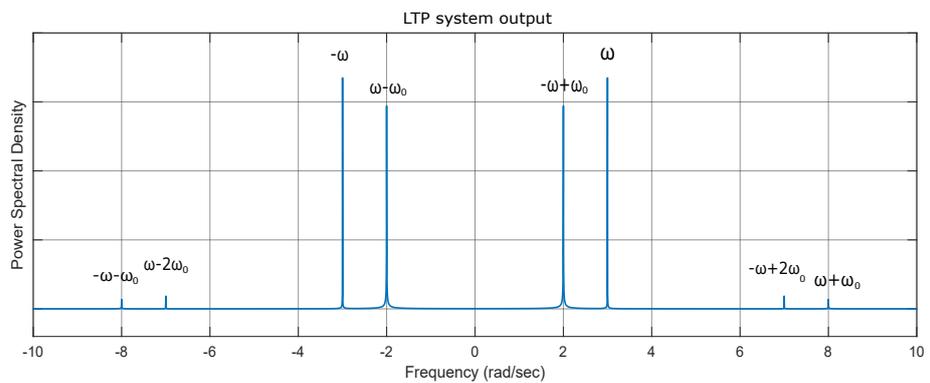
Figure 2.1: Power Spectral Densities of (a) $u = sin(\omega t)$, (b) output of the example LTI system, (c) output of the example LTP system

Substituting equations of (2.21) and (2.22) in the system (2.7) we obtain,

$$\sum_n s_n x_n e^{s_n t} = \sum_n A_n e^{jn\omega_0 t} \sum_m x_m e^{s_m t} + \sum_n B_n e^{jn\omega_0 t} \sum_m u_m e^{s_m t}$$
$$\sum_n y_n e^{s_n t} = \sum_n C_n e^{jn\omega_0 t} \sum_m x_m e^{s_m t} + \sum_n D_n e^{jn\omega_0 t} \sum_m u_m e^{s_m t}$$

$$(2.23)$$

After rearranging the summations and substituting $n = n - m$ in (2.23) we obtain

$$\sum_n s_n x_n e^{s_n t} = \sum_n (\sum_m A_{n-m} x_m + \sum_m B_{n-m} u_m) e^{s_n t}$$
$$\sum_n y_n e^{s_n t} = \sum_n (\sum_m C_{n-m} x_m + \sum_m D_{n-m} u_m) e^{s_n t}$$

$$(2.24)$$

Principle of harmonic balance [31] implies that the equations:

$$s_n x_n = \sum_m A_{n-m} x_m + \sum_m B_{n-m} u_m$$
$$y_n = \sum_m C_{n-m} x_m + \sum_m D_{n-m} u_m$$

$$(2.25)$$

must hold for all $n \in \mathbb{Z}$. The equations in (2.25) represent the relationship between the Fourier coefficients of the input and output signals in a brief manner, however since dealing with summations can be tiresome we are going to write the same equations in doubly infinite matrix equations making use of the Toeplitz transform as:

$$s\mathcal{X} = (\mathcal{A} - \mathcal{N})\mathcal{X} + \mathcal{B}\mathcal{U}$$
$$\mathcal{Y} = \mathcal{C}\mathcal{X} + \mathcal{D}\mathcal{U}$$

$$(2.26)$$

where $\mathcal{X}, \mathcal{U}$ & $\mathcal{Y}$ are vectors comprised of Fourier coefficients of $x(t), u(t)$ *and* $y(t)$

$$\mathcal{X} = \begin{bmatrix} \dots & x_{-2}^T & x_{-1}^T & x_0^T & x_1^T & x_2^T & \dots \end{bmatrix}^T$$
$$\mathcal{U} = \begin{bmatrix} \dots & u_{-2}^T & u_{-1}^T & u_0^T & u_1^T & u_2^T & \dots \end{bmatrix}^T$$
$$\mathcal{Y} = \begin{bmatrix} \dots & y_{-2}^T & y_{-1}^T & y_0^T & y_1^T & y_2^T & \dots \end{bmatrix}^T$$

$$(2.27)$$

and $\mathcal{A}, \mathcal{B}, \mathcal{C}, and \mathcal{D},$ are Toeplitz transforms of $A(t), B(t), C(t), and D(t),$

$$\mathcal{A} = \begin{bmatrix} \ddots & \ddots & \ddots & \ddots & \ddots \\ \ddots & A_0 & A_{-1} & A_{-2} & \ddots \\ \ddots & A_1 & A_0 & A_{-1} & \ddots \\ \ddots & A_2 & A_1 & A_0 & \ddots \\ \ddots & \ddots & \ddots & \ddots & \ddots \end{bmatrix}$$

$$(2.28)$$

etc., and N is a block diagonal matrix in the form

$$\mathcal{N} = \text{blkdiag}\{jn\omega_0 I\}$$

$$= \begin{bmatrix} \ddots & \ddots & \ddots & \ddots & \ddots \\ \ddots & -j\omega_0 I & 0 & 0 & \ddots \\ \ddots & 0 & 0 & 0 & \ddots \\ \ddots & 0 & 0 & -j\omega_0 I & \ddots \\ \ddots & \ddots & \ddots & \ddots & \ddots \end{bmatrix} \quad (2.29)$$

where I is the identity matrix in the same dimension as $A(t)$.

Although, the system in (2.26) is an LTI system fully representing the dynamics of the original LTP system (2.7) it is still not convenient to study using LTI methods due to its infinite dimension. To overcome this difficulty, infinite dimensional matrices of (2.26) need to be truncated to obtain a finite dimensional LTI approximation of the LTP system. This approximation may introduce some errors and convergence issues [40] but these issues are left as a future work in the scope of this thesis.

Another way of expressing LTP systems in an LTI form is *harmonic transfer function* (HTF) concept. HTF's can be derived from the impulse response as well as they can be obtained from the in the state space representation in (2.26), in the same way as LTI systems,

$$H(s) = \mathcal{C}[s\mathcal{I} - (\mathcal{A} - \mathcal{N})]^{-1}\mathcal{B} + \mathcal{D} \quad (2.30)$$

Since there is coupling between harmonics of the input and output signals, $\mathcal{H}(s)$ is again a doubly infinite matrix with each element of it describing the relationship between one harmonic of the input and one harmonic of the output as,

$$\mathcal{Y}(s) = \mathcal{H}(s)\mathcal{U}(s) \quad (2.31)$$

13

where,

$$\mathcal{U}(s) = \begin{bmatrix} \ldots & U(s - j\omega_0) & U(s) & U(s + j\omega_0) & \ldots \end{bmatrix}^T$$

$$\mathcal{Y}(s) = \begin{bmatrix} \ldots & Y(s - j\omega_0) & Y(s) & Y(s + j\omega_0) & \ldots \end{bmatrix}^T$$

$$\mathcal{H}(s) = \begin{bmatrix} \ddots & \ddots & \ddots & \ddots & \ddots \\ \ddots & H_0(s - j\omega_0) & H_{-1}(s) & H_{-2}(s + j\omega_0) & \ddots \\ \ddots & H_1(s - j\omega_0) & H_0(s) & H_{-1}(s + j\omega_0) & \ddots \\ \ddots & H_2(s - j\omega_0) & H_1(s) & H_0(s + j\omega_0) & \ddots \\ \ddots & \ddots & \ddots & \ddots & \ddots \end{bmatrix} \qquad (2.32)$$

Here, $H_0(s)$ is the transfer function between the DC components of the input and output etc.

As with harmonic balance representation (2.26), infinite dimension problem can also be addressed/approximated with truncation.

CHAPTER 3

STATE FEEDBACK CONTROLLER DESIGN BASED ON HARMONIC BALANCE

In Chapter 2, we gave background information regarding linearization of nonlinear systems around periodic orbits and some analysis techniques of LTP systems. In this chapter, we are going to explain our control methodology on an example system using trajectory linearization and harmonic balance approach (2.26).

3.1 Example System

In order to illustrate the principles and properties of our control methodology, we choose the underactuated cart-pendulum system illustrated in Figure 3.1. The cart-pendulum system has highly coupled nonlinear equations of motion. The system has a total of two degrees of freedom (DOF), however it has only 1 actuator which makes the system underactuated. System dynamics are expressed with the equations (3.1) and (3.2).

$$(M_c + M_p)\ddot{x}(t) + M_p l_p cos(\theta(t))\ddot{\theta}(t) - M_p l_p sin(\theta(t))\dot{\theta}^2(t) = F(t) - B_{eq}\dot{x}(t) \qquad (3.1)$$

$$M_p l_p cos(\theta(t))\ddot{x}(t) + (I_p + M_p l_p^2)\ddot{\theta}(t) + M_p g l_p sin(\theta(t)) = -B_p\dot{\theta}(t) - K_s(\theta(t) - \pi) \qquad (3.2)$$

Here, $\theta(t)$ is the deviation of the pendulum angle from the downward vertical in the counter-clockwise direction, $x(t)$ is the horizontal position of the cart and $F(t)$ is the horizontal force acting on the cart. Both $x(t)$ and $F(t)$ are taken positive towards the right hand side. Descriptions of the rest of the variables in equations (3.1) and (3.2) are given in Table 3.1. We borrowed the system parameters from the Quanser's linear servo base unit with inverted pendulum. A rotational spring is attached at the

(a)   (b)
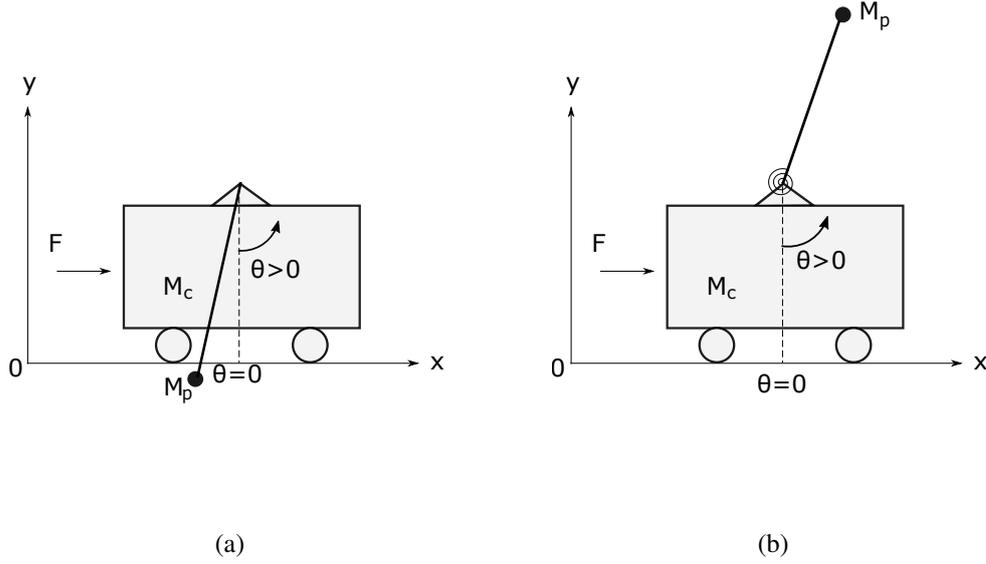
Figure 3.1: (a) Cart-pendulum system (b) Cart-inverted pendulum system with rotational spring

pendulum pivot so that we have control over the degree of instability of the system around the unstable equilibrium point (inverted pendulum case). We have taken the rotational spring constant as 0 for open-loop stable limit cycle analysis (regular pendulum case). We assumed that the pendulum has a point mass at its center and the moment of inertia of the pendulum around its center of gravity is calculated as,

$$I_p = \frac{1}{3} M_p l_p^2 \tag{3.3}$$

Input to the system is taken as the motor voltage $V(t)$. Equation (3.4) gives the relationship between $V(t)$ and $F(t)$.

$$F(t) = -\frac{K_g^2 K_t K_m}{R_m r_{mp}^2} \dot{x}(t) + \frac{K_g K_t}{R_m r_{mp}} V(t) \tag{3.4}$$

By solving the equations (3.1),(3.2) for $\ddot{x}(t)$ and $\ddot{\theta}(t)$ we obtain the equations of motion and analyze the system in a 4 dimensional state space with the states,

$$z(t) = \begin{bmatrix} z_1(t) & z_2(t) & z_3(t) & z_4(t) \end{bmatrix}^T = \begin{bmatrix} x(t) & \theta(t) & \dot{x}(t) & \dot{\theta}(t) \end{bmatrix}^T \tag{3.5}$$

which are assumed to be fully observable, and state space representation,

16

$$\dot{z}(t) = f(z(t), u(t)) = \begin{bmatrix} z_3(t) & z_4(t) & f_3(z(t), u(t)) & f_4(z(t), u(t)) \end{bmatrix}^T$$

$$y(t) = \begin{bmatrix} 1 & 0 & 0 & 0 \\ 0 & 1 & 0 & 0 \\ 0 & 0 & 0 & 0 \\ 0 & 0 & 0 & 0 \end{bmatrix} z(t) \tag{3.6}$$

Table 3.1: Cart-pendulum variables

Symbol	Description	Value	Unit
M_c	Weight of the cart	0.57	kg
M_p	Weight of the pendulum	0.21	kg
l_p	Pendulum half length	0.3	m
B_{eq}	Equivalent viscous damping coefficient at the motor pinion	4.3	$N \cdot s/m$
I_p	Pendulum moment of inertia	0.0063	$kg \cdot m^2$
g	Gravitational acceleration	9.8	m/s^2
B_p	Pendulum damping coefficient	0.05	$N \cdot m \cdot s/rad$
K_s	Rotational spring coefficient	0.74/0	$N \cdot m/rad$
K_g	Planetary gearbox ratio	3.71	
K_t	Motor torque constant	0.00767	$N \cdot m/A$
K_m	EMF constant	0.00767	$V \cdot s/rad$
R_m	Motor armature resistance	2.6	Ω
r_{mp}	Motor pinion radius	6.35×10^{-3}	m

3.2 Open-Loop Controller

We assume there exist a set of periodic trajectories $\{z_0(t),\ u_0(t)\}$ that solves (3.1) and (3.2). In this context, we define a reference sinusoidal trajectory for the position of the cart *or* the pendulum angle. Since the system is underactuated, we can define the reference trajectory only for one variable, and the trajectory for the other variable is a by product of dynamical interactions. For this reason, we substitute the determined reference trajectory for the chosen coordinate variable and then solve the equation (3.2) via numerical integration to obtain a solution for the remaining variable at steady state. In general, this periodic solution includes the selected baseline frequency as
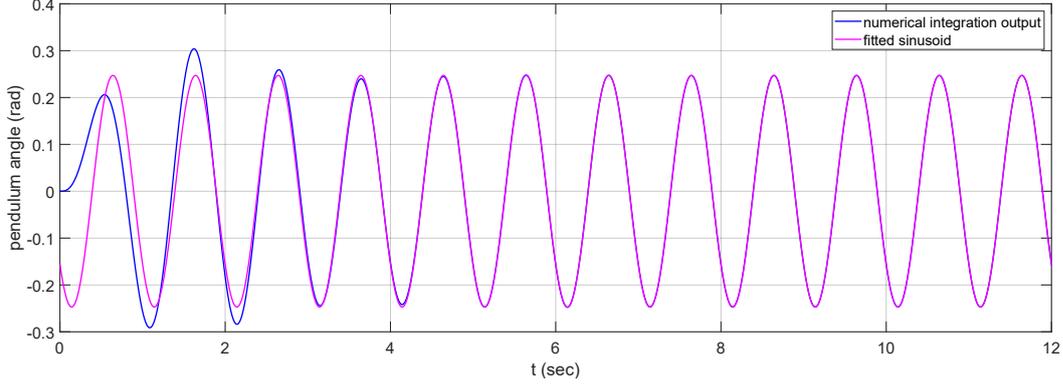
Figure 3.2: Solution of the input independent dynamic equation (3.2) for position reference with rotational spring coefficient $K_s = 0$

well as its harmonics. However, our observations show that harmonics in the resultant trajectories are negligible. Thus, we fit a sinusoid to the output of the numerical integration and obtain an analytical expression for the second "reference" trajectory.

For example, assume a reference trajectory for cart position as:

$$x(t) = 5 \times 10^{-2} \sin(2\pi t) \ m \tag{3.7}$$

Solving (3.2) after substituting the second derivative of (3.7) and fitting a sinusoid yields the following expression

$$\theta(t) = -0.2472 \sin(2\pi t + 0.6809) \ rad \tag{3.8}$$

The numerical solution and the fitted sinusoid for pendulum angle are illustrated in figure 3.2. As expected, the analytic expression shares the same frequency with the position reference, however with a phase difference. We obtain the reference trajectories for the remaining system states–the translational velocity of the cart and the angular velocity of the pendulum–through differentiation.

Once we have the reference trajectories for the states $z_0(t)$ we can substitute these in equation (3.1) and obtain an analytical expression for the input $u_0(t) = V_0(t)$.

For the example trajectories of (3.7) and (3.8), open-loop input is derived as,

$$u_0(t) = V_0(t) = 2.2894 \sin(2\pi t + 2.2095) \ V \tag{3.9}$$

When this calculated sinusoid (3.9) is input to the system, system states through the numerical solution of (3.6) are obtained as illustrated in figure 3.3.
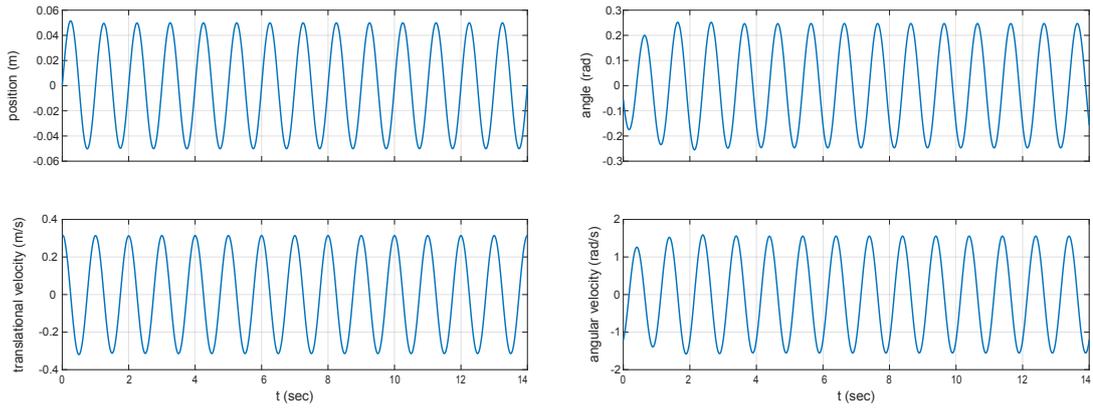
Figure 3.3: System response to open-loop input

3.3 State Feedback Controller

In Section 3.2, we numerically showed the existence of periodic solutions for the cart-pendulum system. However, this periodic-orbit (or limit-cycle) may be unstable or the convergence behavior may be not satisfactory. At this point our main concern is designing a parallel add-on feedback controller, $u_f(t)$, to improve the stability of these periodic solutions, which are assumed to be controllable. In addition to stabilization around the periodic-orbit, we require the feedback control policy to track possible changes in the reference trajectory. Figure 3.4 demonstrates the overall closed loop system structure.
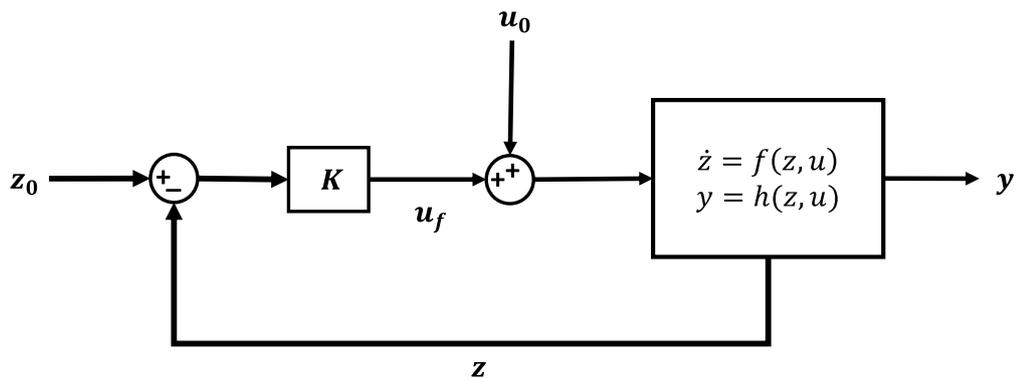
Figure 3.4: Overall control structure

3.3.1 Trajectory Linearization

Before designing the state feedback controller, we first linearize the system around the pre-defined periodic solution $\{z_0(t),\ u_0(t)\}$ according to the scheme provided in Section 3.2. As a result of this linearization we obtain the following LTP system structure,

$$
\dot{z}(t) = \underbrace{\begin{bmatrix} 0 & 0 & 1 & 0 \\ 0 & 0 & 0 & 1 \\ 0 & a_{32} = \frac{\partial f_3(z,u)}{\partial z_2} & a_{33} = \frac{\partial f_3(z,u)}{\partial z_3} & a_{34} = \frac{\partial f_3(z,u)}{\partial z_4} \\ 0 & a_{42} = \frac{\partial f_4(z,u)}{\partial z_2} & a_{43} = \frac{\partial f_4(z,u)}{\partial z_3} & a_{44} = \frac{\partial f_4(z,u)}{\partial z_4} \end{bmatrix}}_{A(t)} z(t)
$$

$$
+ \underbrace{\begin{bmatrix} 0 \\ 0 \\ b_3 = \frac{\partial f_3(z,u)}{\partial u} \\ b_4 = \frac{\partial f_4(z,u)}{\partial u} \end{bmatrix}}_{B(t)} u(t) \tag{3.10}
$$

$$
y(t) = \underbrace{\begin{bmatrix} 1 & 0 & 0 & 0 \\ 0 & 1 & 0 & 0 \\ 0 & 0 & 1 & 0 \\ 0 & 0 & 0 & 1 \end{bmatrix}}_{C(t)} z(t)
$$

Figures 3.5 and 3.6 demonstrate the power spectral densities of the elements of system matrices $A(t)$ and $B(t)$, for limit cycles around the stable and unstable equilibrium points, respectively. For the stable equilibrium, linearization is performed around a limit cycle with position reference trajectory $x(t) = 0.05\sin(2\pi t)\ m$ and for unstable equilibrium, linearization is performed around a limit-cycle with pendulum angle reference trajectory $\theta(t) = \pi + 0.1\sin(10\pi t)\ rad$. Expectedly, the most dominant components are DC (LTI) components for both cases. However we observe operationally significant power at the second harmonic especially for inverted pendulum case in a_{32} and a_{42} components.

20
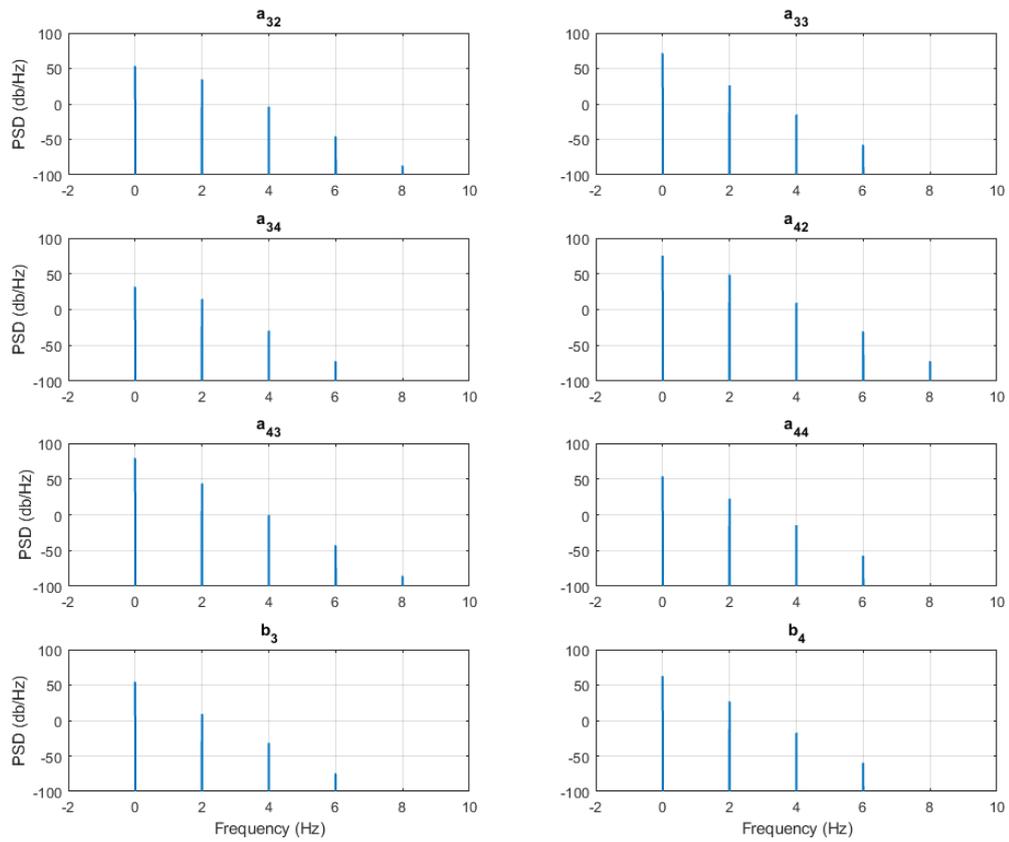
Figure 3.5: Power Spectral Densities of the elements of LTP system matrices $A(t)$ and $B(t)$ for linearization around a limit cycle around the stable equilibrium point with fundamental frequency $\omega_0 = 2\pi \ rad/s$
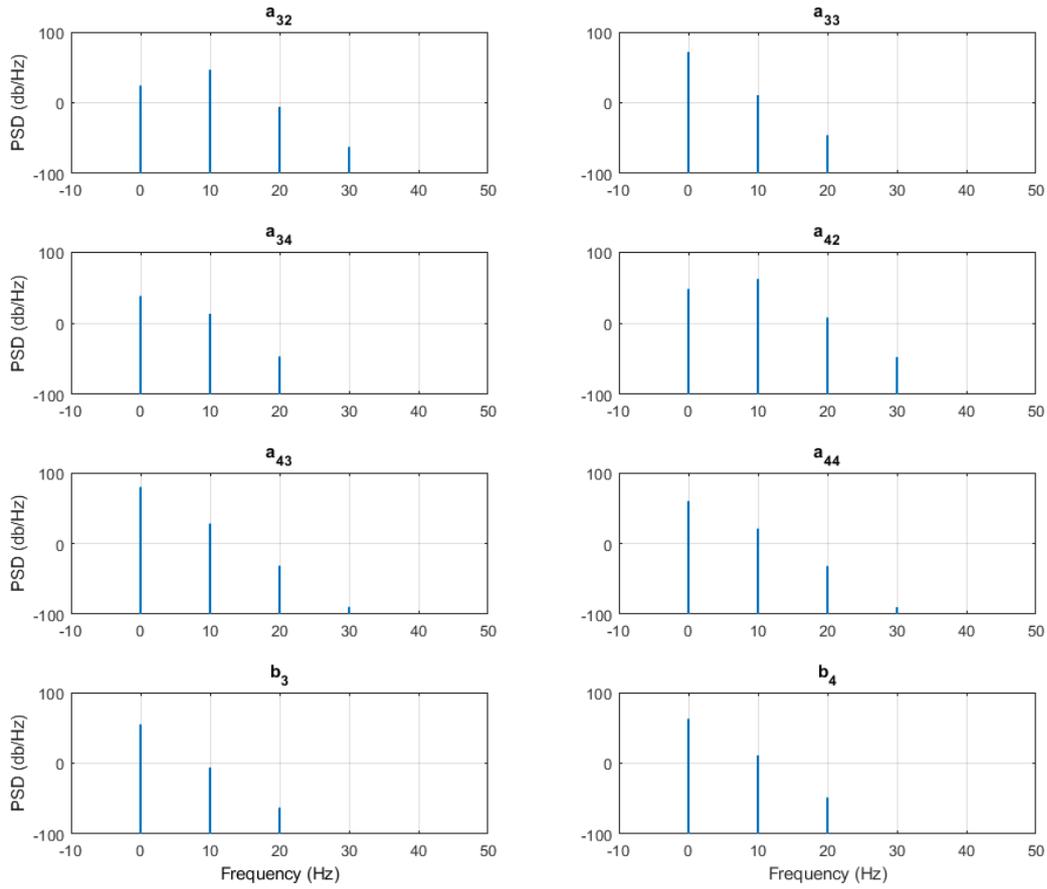
Figure 3.6: Power Spectral Densities of the elements of LTP system matrices $A(t)$ and $B(t)$ for linearization around a limit cycle around the unstable equilibrium point with fundamental frequency $\omega_0 = 10\pi \ rad/s$

3.3.2 Truncated Toeplitz Transform

In our approach, after the linearization phase, we bring the system into the harmonic balance form proposed in equation (2.26). In this direction, we need to compute the Fourier series coefficients of the matrices $A(t)$ and $B(t)$. One should also note the fact that $C(t) = I$ is a constant matrix. In other words, we assume that we can measure all system states [37].

Since only the DC component and second harmonic at $2\omega_0$ have noticeable effect in the LTP formulation, we truncated the Toeplitz matrix such that we have 4×4 A_i blocks in the truncated form for computational purposes. Note that theoretically, except for pure LTI case, Toeplitz matrix has to be infinite dimensional for exact formulation. In the future, we will test different level of truncations and their effect on closed-loop control performance. As a result, in the harmonic balance form, we have $4 \times 5 = 20$ states

$$\mathcal{Z} = \begin{bmatrix} z_{-2}^T & z_{-1}^T & z_0^T & z_1^T & z_2^T \end{bmatrix}^T \tag{3.11}$$

and system matrices in the form:

$$\mathcal{A} = \begin{bmatrix} A_0 & A_{-1} & A_{-2} & A_{-3} & A_{-4} \\ A_1 & A_0 & A_{-1} & A_{-2} & A_{-3} \\ A_2 & A_1 & A_0 & A_{-1} & A_{-2} \\ A_3 & A_2 & A_1 & A_0 & A_{-1} \\ A_4 & A_3 & A_2 & A_1 & A_0 \end{bmatrix} \tag{3.12}$$

where $\mathcal{A} \in \mathbb{C}^{20 \times 20}$ and $\mathcal{B} \in \mathbb{C}^{20 \times 5}$.

3.3.3 Eigenvalue Optimization

For LTP systems, eigenvalues of the infinite dimensional system matrix in Toeplitz form, $\mathcal{A} - \mathcal{N}$ characterizes the stability of the system. In our case, If the truncation errors are negligible, and if the system trajectories stays in the close proximity of the limit-cycle, eigenvalues of the truncated system matrix in Toeplitz form, $\mathcal{A} - \mathcal{N}$, provide local stability information to some accuracy. In this context, we can design

a state feedback controller to make the closed-loop system asymptotically stable by placing the eigenvalues of the matrix:

$$\mathcal{A}_{cl} = \mathcal{A} - \mathcal{N} - \mathcal{B}\mathcal{K}_{\mathcal{T}} \tag{3.13}$$

to the open left half of the complex plane. In equation (3.13) K_T is the Toeplitz transform of the feedback vector K. Since K is LTI, $\mathcal{K}_{\mathcal{T}} \in \Re^{5 \times 20}$ is a block diagonal matrix expressed as

$$\mathcal{K}_{\mathcal{T}} = \begin{bmatrix} K & & & & \\ & K & & \mathbf{0} & \\ & & K & & \\ & \mathbf{0} & & K & \\ & & & & K \end{bmatrix} \tag{3.14}$$

As a result of the multiplication of truncated Toeplitz matrices of $B(t)$ and K, the same feedback coefficient will affect each harmonic of $B(t)$ as,

$$\mathcal{B}\mathcal{K}_{\mathcal{T}} = \begin{bmatrix} B_0 K & B_{-1} K & \ldots \\ B_1 K & B_0 K & \ldots \\ \vdots & \vdots & \ddots \end{bmatrix}, \tag{3.15}$$

For the system in truncated harmonic balance form, it is not possible to implement pole placement directly since we have 4 measurable states, i.e. 4 dimensional state-feedback vector, and a 20 dimensional "system". Instead we employ optimization methods to place the truncated LTP system poles such that the nonlinear system is asymptotically stable.

Dynamics of the inverted and downward pendulum cases are significantly different. Hence, behavior of the eigenvalues of $\mathcal{A}_{cl}$ with respect to K is quite different as well. For this reason, we needed to apply different optimization methods (and constrains) for two cases.

For downward pendulum case to solve the problem,

$$K = \underset{K \in \Re^4}{\arg\min}(\max(real(eigen(\mathcal{A}_{cl}))))$$
$$\text{subject to}: -\min(real(eigen(\mathcal{A}_{cl}))) - 50 < 0 \tag{3.16}$$

24

we use a nonlinear programing solver. Real part of the maximum eigenvalue is minimized to increase the convergence speed and real part of the minimum eigenvalue is limited from the left to keep the control input at reasonable levels. This method works well on this case since the objective function $f(K) = \max(real(eigen(\mathcal{A}_{cl})))$ changes smoothly with changing K as can be seen in figure 3.7.

Figure 3.7: Change in the real part of maximum eigenvalue of $\mathcal{A}_{cl}$ with respect to K for downward pendulum case

As for inverted pendulum case we solve the problem,

$$K = \underset{K \in \Re^4}{\arg\min}(\max(real(eigen(\mathcal{A}_{cl}))))$$

$$\text{subject to}: \ 10^7 - KQK^T < 0$$

$$KRK^T - 50 < 0 \tag{3.17}$$

$$\max(real(eigen(\mathcal{A}_{cl}))) + 15 < 0$$

where

$$Q = \begin{bmatrix} 10 & 0 & 0 & 0 \\ 0 & 1 & 0 & 0 \\ 0 & 0 & 0 & 0 \\ 0 & 0 & 0 & 0 \end{bmatrix}, \ R = \begin{bmatrix} 0 & 0 & 0 & 0 \\ 0 & 1 & 0 & 0 \\ 0 & 0 & 1 & 0 \\ 0 & 0 & 0 & 10 \end{bmatrix} \tag{3.18}$$

again using a nonlinear programming solver but inside a particle swarm optimization algorithm. We utilized a swarm intelligence algorithm since the objective function for this case, as can be seen in figure 3.8, has some local minima and its gradient is

too small for most K that the classical algorithms fail to find a feasible solution. Real part of the maximum eigenvalue has again been chosen as the objective function in order to increase the convergence rate and some extra constraints are included based on our observations regarding the system behavior. 3rd and 4th elements of K are coefficients of the velocities and they need to be small since the system unstable and quite susceptible to noise and uncertainties. First two elements of K need to be high in order to robustly stabilize the system. First element of K, which is the feedback gain of the cart position, is kept higher since the system is underactuated and we do not have direct control over pendulum angle. Finally, a constraint is imposed on the real part of the minimum eigenvalue also to increase the system speed. For this system configuration, we did not impose a left limit since the eigenvalues did not converge towards infinity for the feedback gain values that made the system stable.
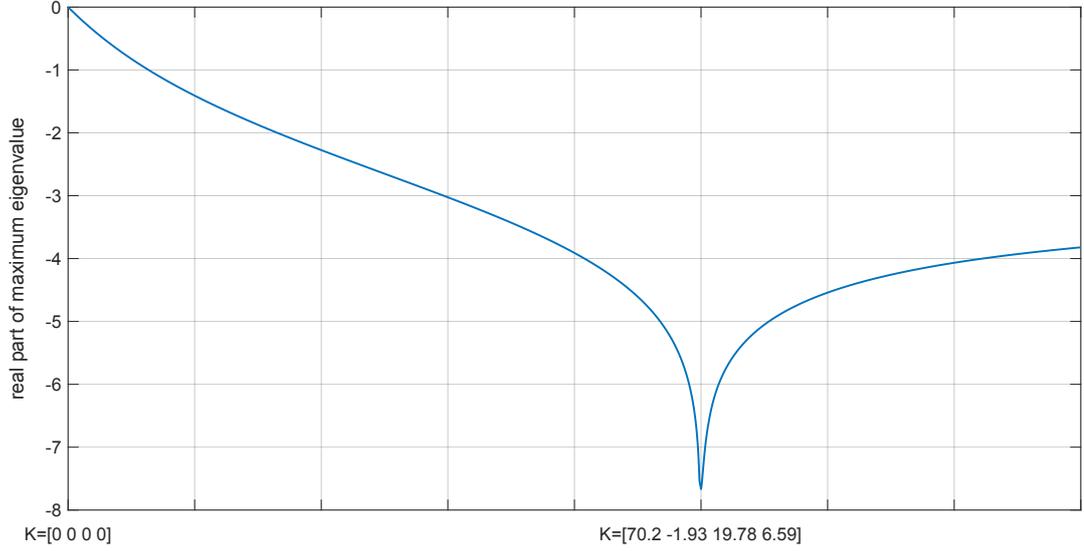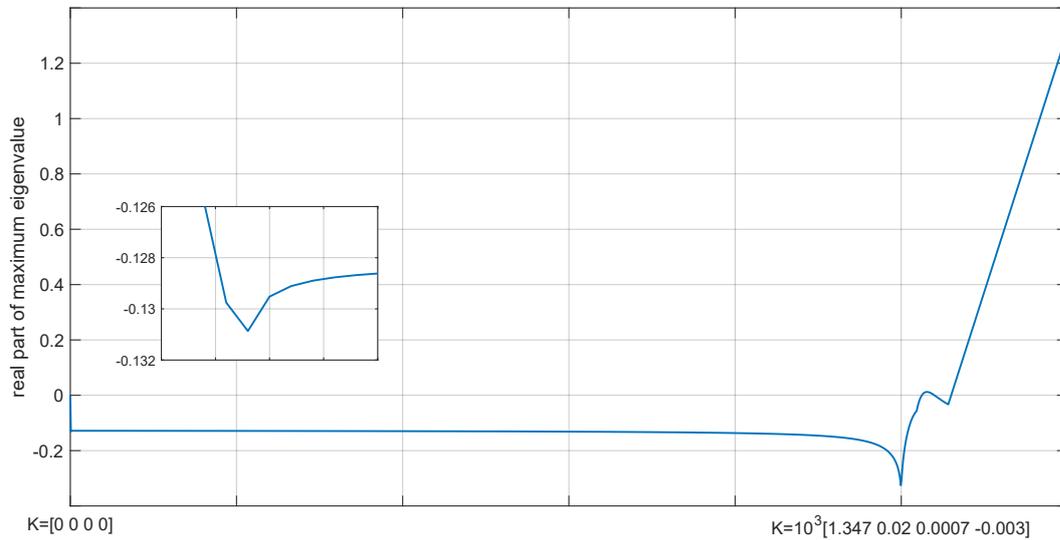

Figure 3.8: Change in the real part of maximum eigenvalue of $\mathcal{A}_{cl}$ with respect to K for inverted pendulum case

In figures (3.7) and (3.8) indicated values of K are two solutions of the given optimization problem and change in K is linear.

26

Algorithm 1 Particle Swarm Optimization

1: **for** k=1:SwarmSize **do**
2:     $K(k,:) = 1000 * randn(1,4)$
3:     $K(k,:) = nonlinear\_programing\_solver(K(k,:))$
4:     $v(k,:) = randn(1,4)$
5:     $f_b(k) = objective function(K(k,:))$
6:     $K_{best}(k,:) = K(k,:)$
7:     **if** $f_b(k) < f_{best}$ **then**
8:         $f_{best} = f_b(k)$
9:         $K_{gbest} = K(k,:)$
10:    **end if**
11: **end for**
12: **for** j=1:NumberofIterations **do**
13:     **for** k=1:SwarmSize **do**
14:         $v(k,:) = v(k,:) + randn(1,n)(Kbest(k,:) - K(k,:)) + randn(1,n)(K_{gbest} - K(k,:))$
15:         $K(k,:) = K(k,:) + v(k,:)$
16:         $K(k,:) = nonlinear\_programing\_solver(K(k,:))$
17:         $f(k) = objective function(K(k,:))$
18:         **if** $f(k) < f_b(k)$ & constraints satisfied **then**
19:             $f_b(k) = f(k)$
20:             $K_{best(k,:)} = K(k,:)$
21:             **if** $f(k) < f_{best}$ **then**
22:                 $f_{best} = f(k)$
23:                 $K_{gbest} = K(k,:)$
24:             **end if**
25:         **end if**
26:     **end for**
27: **end for**
28: **return** K_{gbest}

CHAPTER 4

RESULTS AND DISCUSSION

We applied the controller design procedures proposed in Section 3.3 on the example system given in Section 3.1 in simulation environment. In this section, we will provide the simulation results and draw some conclusions.

4.1 Downward Pendulum

We first analyze the system, when the pendulum oscillates around its stable equilibrium point. For this case rotational spring coefficient is $K_s = 0$.

4.1.1 Open-Loop Behavior

If we ignore the horizontal position of the cart and consider only the cart velocity, pendulum angle and its derivative, open-loop system exhibits asymptotically stable limit cycles for this case. Note that since there is no feedback from the cart position, if we include it as a state the system becomes "marginally stable". This can be observed from the eigenvalues of the approximated LTP system representation in harmonic balance form detailed in Table 4.1. System has 4 eigenvalues at each 2π strip, since the fundamental frequency of the system is $\omega_0 = 2\pi \ rad/s$. 3 of the 4 eigenvalues that are on the fundamental strip has negative real parts have negative real parts and the remaining one is located at the origin.

Remember from linearization around an equilibrium point that if an eigenvalue of the linearized system is zero we cannot comment on the stability of the nonlinear

system based on the eigenvalues of the LTI system, since non-linear terms determine the stability in this direction. However, this does not hold in this example, since the eigenvalue at the origin purely comes from the (linear) integrator term that is existent in the dynamics of the system.

Table 4.1: Open-loop eigenvalues of the truncated LTI approximation for a limit cycle around the stable equilibrium with frequency $\omega_0 = 2\pi \ rad/s$

0.0000 +12.5664i	-1.1370 + 7.8612i	-1.1375 +17.2709ii	-19.3625 +12.5658i
0.0000 + 6.2832i	-1.1370 + 1.5780i	-1.1375 +10.9877i	-19.3625 + 6.2826i
0.0000 + 0.0000i	-1.1373 - 4.7049i	-1.1373 + 4.7049i	-19.3624 - 0.0000i
0.0000 - 6.2832i	-1.1370 - 1.5780i	-1.1375 -10.9877ii	-19.3625 - 6.2826i
0.0000 -12.5664i	-1.1370 - 7.8612i	-1.1375 -17.2709i	-19.3625 -12.5658i

As we can see in Figure 4.1 the LTI part of the LTP system (A_0) and the eigenvalues of the open-loop LTP system in harmonic balance form in the primary frequency strip are almost the same. So we can say that for the open-loop system, A_0 term is mostly dominant.
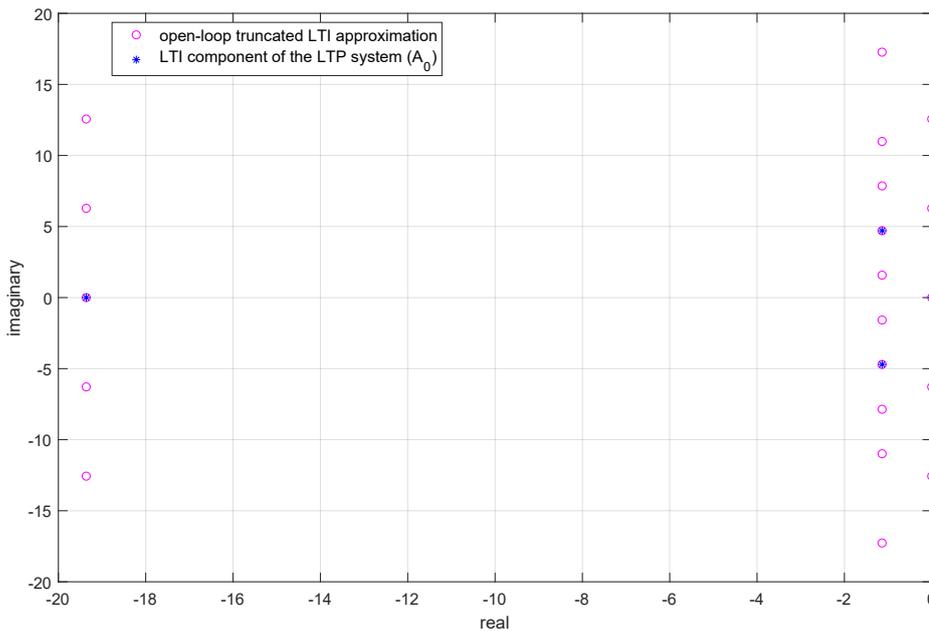
Figure 4.1: Open-loop eigenvalues of the truncated LTI approximation and the LTI component of the LTP system for a limit cycle around the stable equilibrium with frequency $\omega_0 = 2\pi \ rad/s$

As can be seen in figure 4.2 system with only open-loop controller converges to the reference trajectory for pendulum angle at around 3 seconds from zero initial con-

ditions but we need a feedback control structure to track the position trajectory and enhance the system performance.
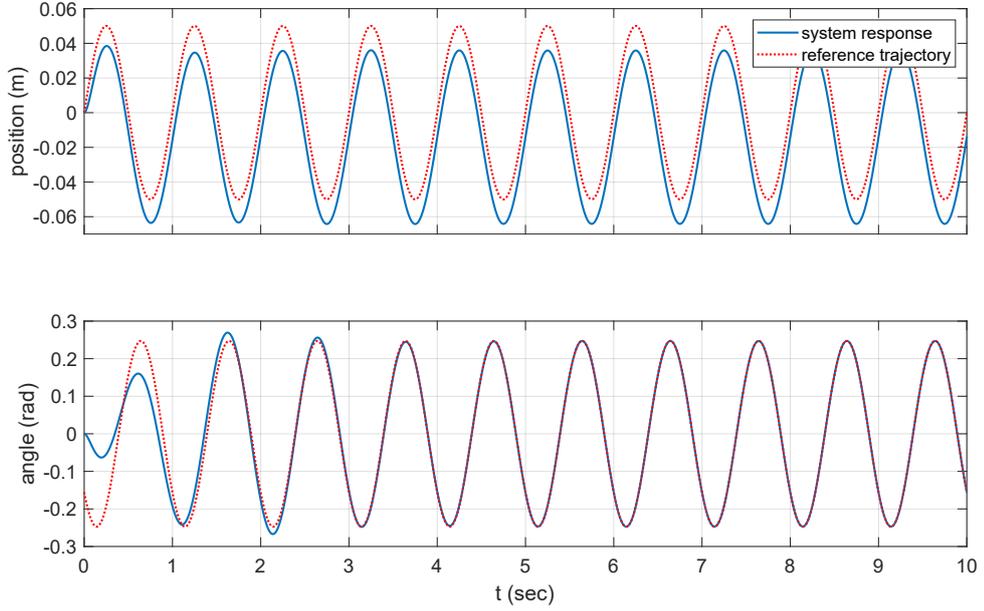
Figure 4.2: Open-loop controlled response of the original nonlinear system around a stable limit cycle with frequency $\omega_0 = 2\pi \ rad/s$ to zero initial conditions

4.1.2 Closed-Loop Behavior

If we solve the optimization problem presented in Section 3.3.3 with different initial conditions for the trajectory,

$$x(t) = 5 \times 10^{-2} \sin(2\pi t) \ m$$
$$\theta(t) = -0.2472 \sin(2\pi t + 0.6809) \ rad$$

(4.1)

we obtain different but similar feedback vectors and closed-loop behaviors are generally very close. Figures 4.3, 4.4 and 4.5 show the system's response from initial conditions $\begin{bmatrix} x & \theta & \dot{x} & \dot{\theta} \end{bmatrix} = \begin{bmatrix} 0.02 \ m & 0.2 \ rad & 0 & 0 \end{bmatrix}$ (deviations from the reference trajectory). Steady state error converges to zero in about 1.2 sec.

31

Figure 4.3: Feedback controlled system response around the stable limit cycle 4.1 with frequency $\omega_0 = 2\pi \ rad/s$ with initial conditions deviating $[x \ \theta \ \dot{x} \ \dot{\theta}] = [0.02 \ m \ 0.2 \ rad \ 0 \ 0]$ from the limit cycle and K = [69.69 -2.01 19.62 6.54]

Figure 4.4: Error of the feedback controlled system response around the stable limit cycle 4.1 with frequency $\omega_0 = 2\pi \ rad/s$ with initial conditions deviating $[x \ \theta \ \dot{x} \ \dot{\theta}] = [0.02 \ m \ 0.2 \ rad \ 0 \ 0]$ from the limit cycle and K = [69.69 -2.01 19.62 6.54]

Figure 4.5: Feedback controlled trajectory around the stable limit cycle 4.1 with frequency $\omega_0 = 2\pi \ rad/s$ with initial conditions deviating $[x \ \theta \ \dot{x} \ \dot{\theta}] = [0.02 \ m \ 0.2 \ rad \ 0 \ 0]$ from the limit cycle and K = [69.69 -2.01 19.62 6.54]

For the closed-loop system, as can be seen in figure 4.6, all the eigenvalues of the LTP system in harmonic balance form are on the open left half plane. We also observe here that the eigenvalues of the closed-loop LTP system and the eigenvalues of $A_0 - B_0K$ part significantly different in closed-loop case. Thus, we observe that even if A_0 component of the open-loop system is dominant in the $\mathcal{A}_{ol}$ matrix, designed feedback controller utilizes the harmonics of the system and eventually dominance of LTI component in the $\mathcal{A}_{cl}$ matrix becomes obsolete.
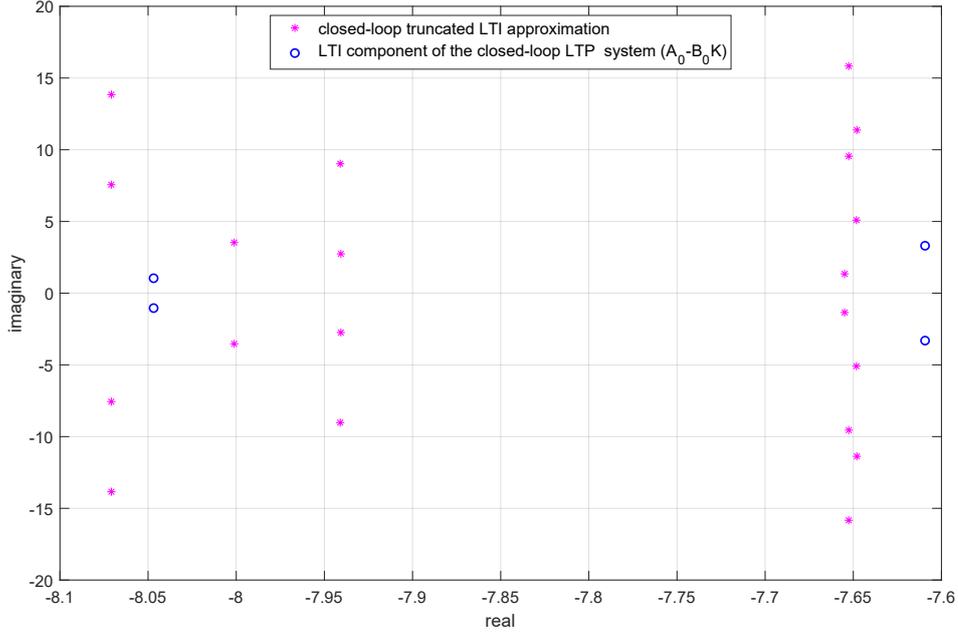
Figure 4.6: Closed-loop eigenvalues of the truncated LTI approximation and the LTI component of the closed-loop LTP system $(A_0 - B_0 K)$ for a limit cycle around the stable equilibrium with frequency $\omega_0 = 2\pi \; rad/s$ and K = [69.69 -2.01 19.62 6.54]

We also test the controller design procedure around different limit cycles and show that the design procedure works for different frequencies and amplitudes of trajectories. As an example we decrease the frequency to 0.8 Hz and increase the amplitude of the position reference to obtain the trajectory,

$$x(t) = 6 \times 10^{-2} \sin(1.6\pi t) \; m$$
$$\theta(t) = -0.3706 \sin(1.6\pi t + 1.449) \; rad$$

(4.2)

and we observe in figures 4.7, 4.8 and 4.9 that we can use the same controller design procedure for stabilization around different limit cycles.
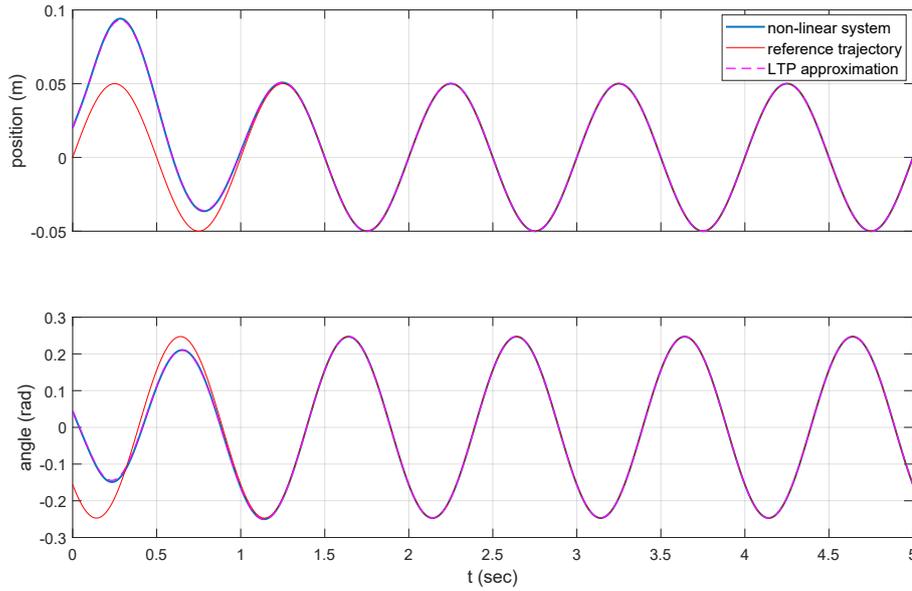
Figure 4.7: Feedback controlled system response around the stable limit cycle 4.2 with frequency $\omega_0 = 1.6\pi\ rad/s$ with initial conditions deviating $[x\ \theta\ \dot{x}\ \dot{\theta}] = [0.02\ m\ 0.2\ rad\ 0\ 0]$ from the limit cycle and K = [75.34 2.01 19.61 6.89]
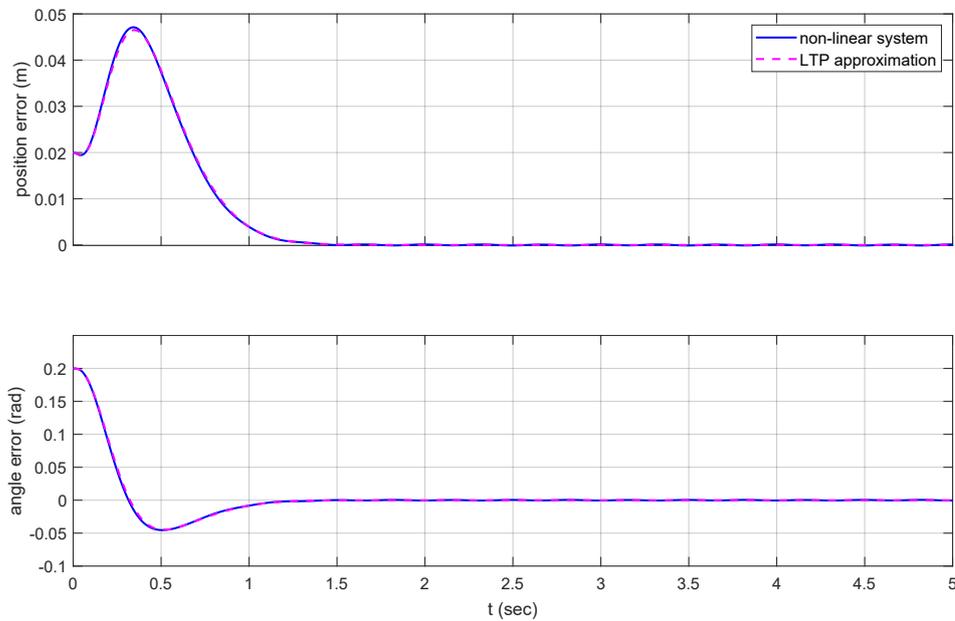

Figure 4.8: Error of the feedback controlled system response around the stable limit cycle 4.2 with frequency $\omega_0 = 1.6\pi\ rad/s$ with initial conditions deviating $[x\ \theta\ \dot{x}\ \dot{\theta}] = [0.02\ m\ 0.2\ rad\ 0\ 0]$ from the limit cycle and K = [75.34 2.01 19.61 6.89]
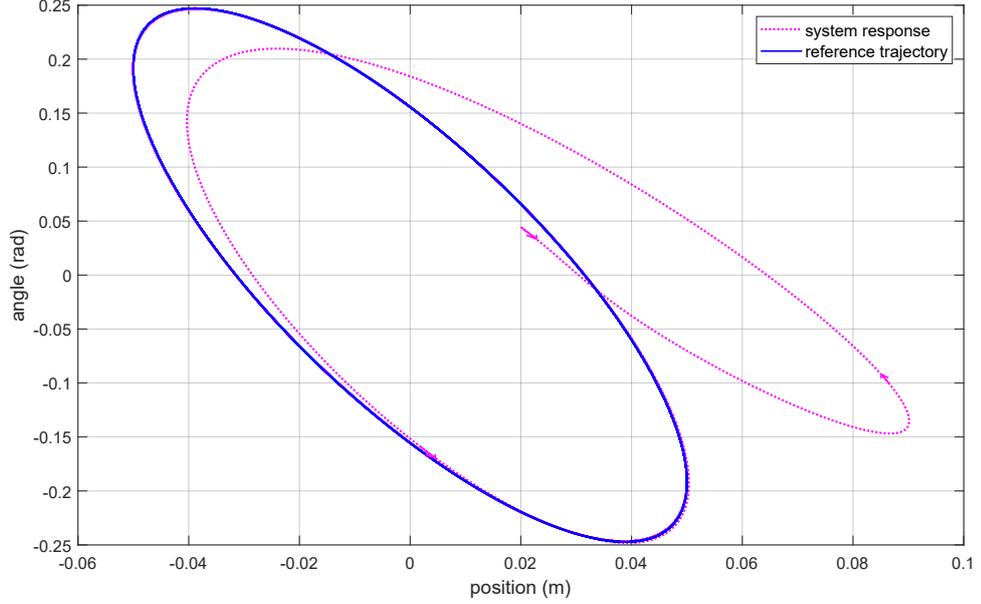
Figure 4.9: Feedback controlled trajectory around the stable limit cycle 4.2 with frequency $\omega_0 = 1.6\pi \ rad/s$ with initial conditions deviating $\begin{bmatrix} x & \theta & \dot{x} & \dot{\theta} \end{bmatrix} = [0.02 \ m \ 0.2 \ rad \ 0 \ 0]$ from the limit cycle and K = [75.34 2.01 19.61 6.89]

4.1.3 Step Response: Cart Position

Figures 4.10, 4.11 and 4.12 demonstrate that the controller can also track changes in the cart position. This can be considered as analogous to adjusting the lateral position in running and walking.

36
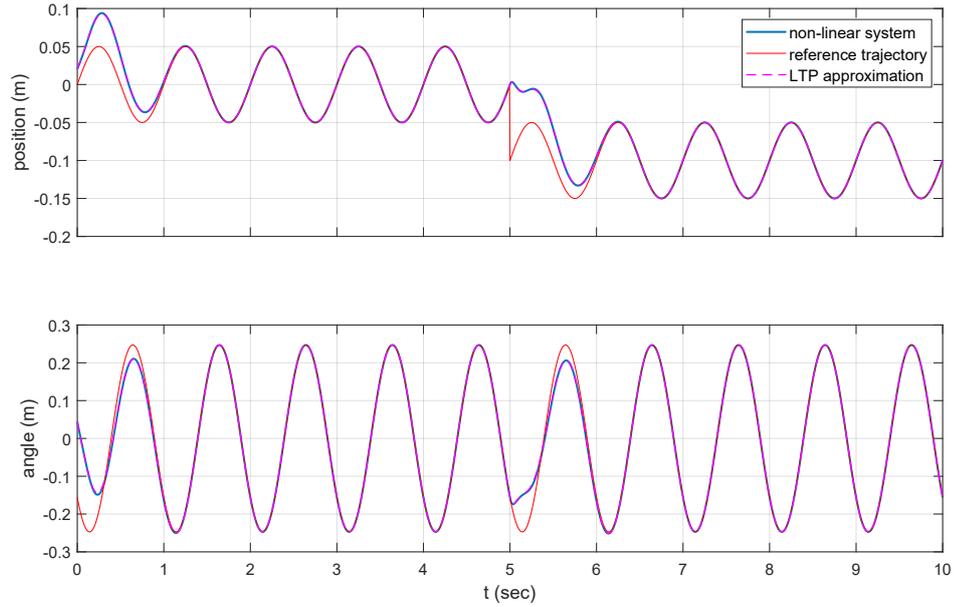
Figure 4.10: Feedback controlled system response around the stable limit cycle 4.1 with frequency $\omega_0 = 2\pi \ rad/s$ with initial conditions deviating $[x \ \theta \ \dot{x} \ \dot{\theta}] = [0.02 \ m \ 0.2 \ rad \ 0 \ 0]$ from the limit cycle, K = [70.29 -1.86 19.78 6.6] and a position step input of -0.1 m
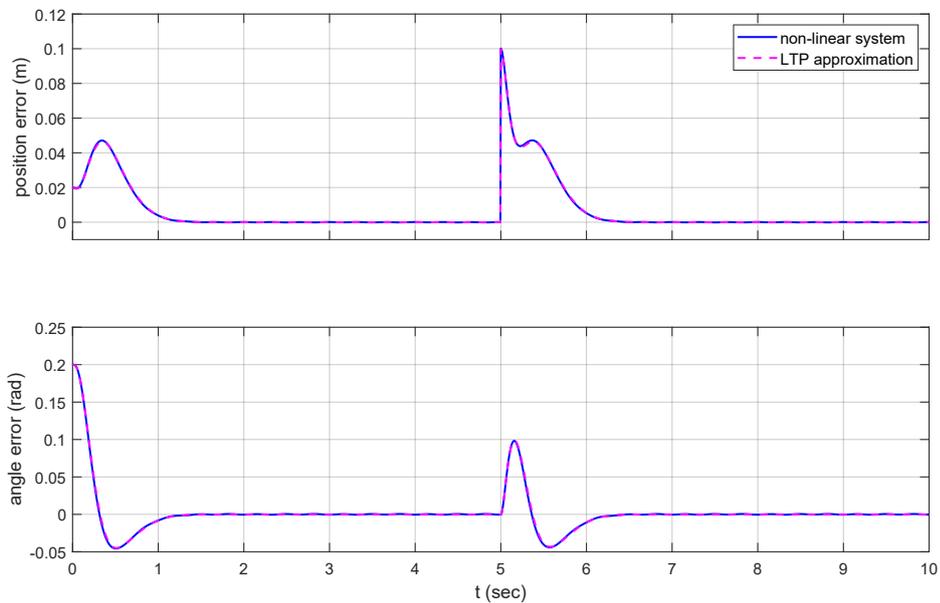
Figure 4.11: Error of the feedback controlled system response around the stable limit cycle 4.1 with frequency $\omega_0 = 2\pi \ rad/s$ with initial conditions deviating $[x \ \theta \ \dot{x} \ \dot{\theta}] = [0.02 \ m \ 0.2 \ rad \ 0 \ 0]$ from the limit cycle, K = [70.29 -1.86 19.78 6.6] and a position step input of -0.1 m
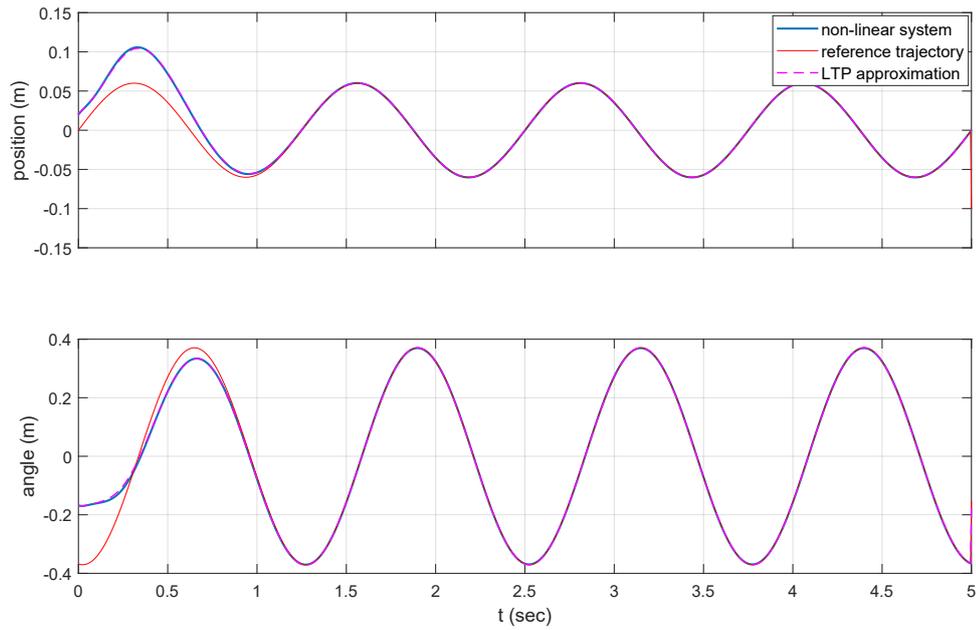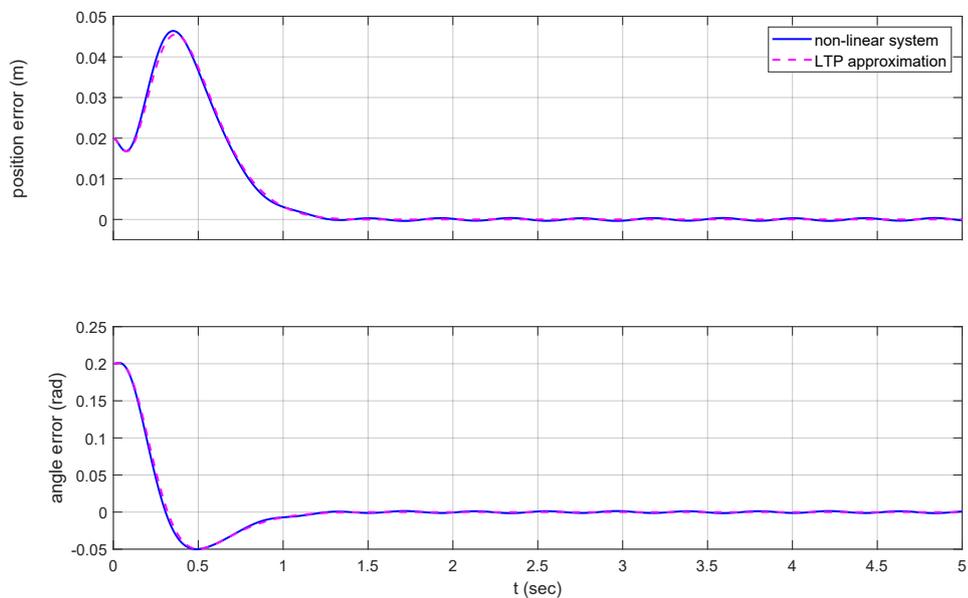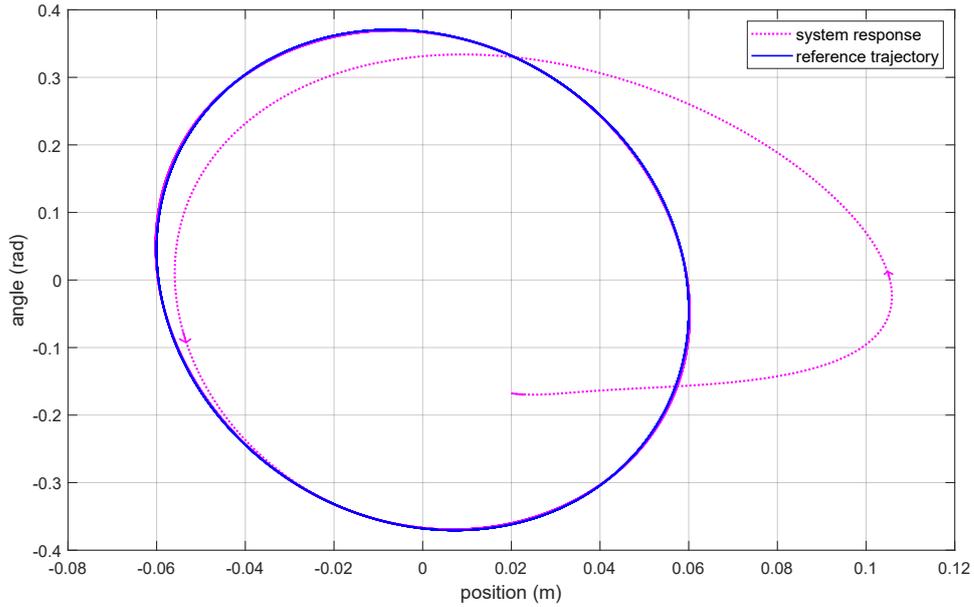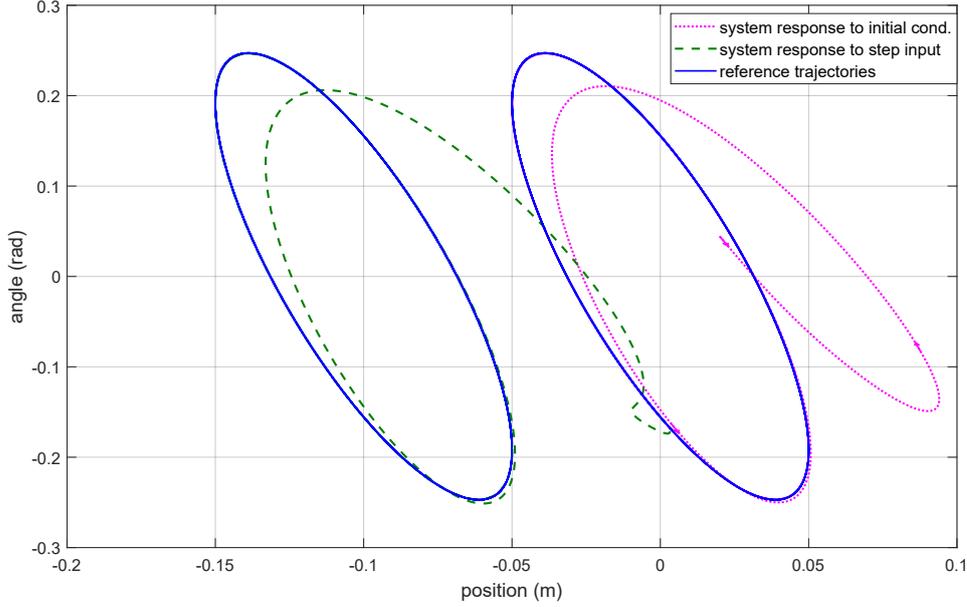
Figure 4.12: Feedback controlled trajectory around the stable limit cycle 4.1 with frequency $\omega_0 = 2\pi \ rad/s$ with initial conditions deviating $[x \ \theta \ \dot{x} \ \dot{\theta}] = [0.02 \ m \ 0.2 \ rad \ 0 \ 0]$ from the limit cycle, K = [70.29 -1.86 19.78 6.6] and a position step input of -0.1 m

4.1.4 Step Response: Limit Cycle Amplitude

In this section we analyze the system undergoing limit cycle amplitude change during the execution of control task. This can be considered as analogous to increasing the step size during walking or running. We change the reference trajectory from (4.1) to (4.3) without changing the open-loop input as can be seen in figure 4.16.

$$x(t) = 7 \times 10^{-2} \sin(2\pi t) \ m$$
$$\theta(t) = -0.3387 \sin(2\pi t + 0.6691) \ rad$$

(4.3)

Linearizing the system around the trajectory (4.1) and designing the open-loop and closed-loop controllers accordingly we see that we can control the system around a much wider limit cycle with a maximum position error around %8 and a maximum angle error around %8.5.

38
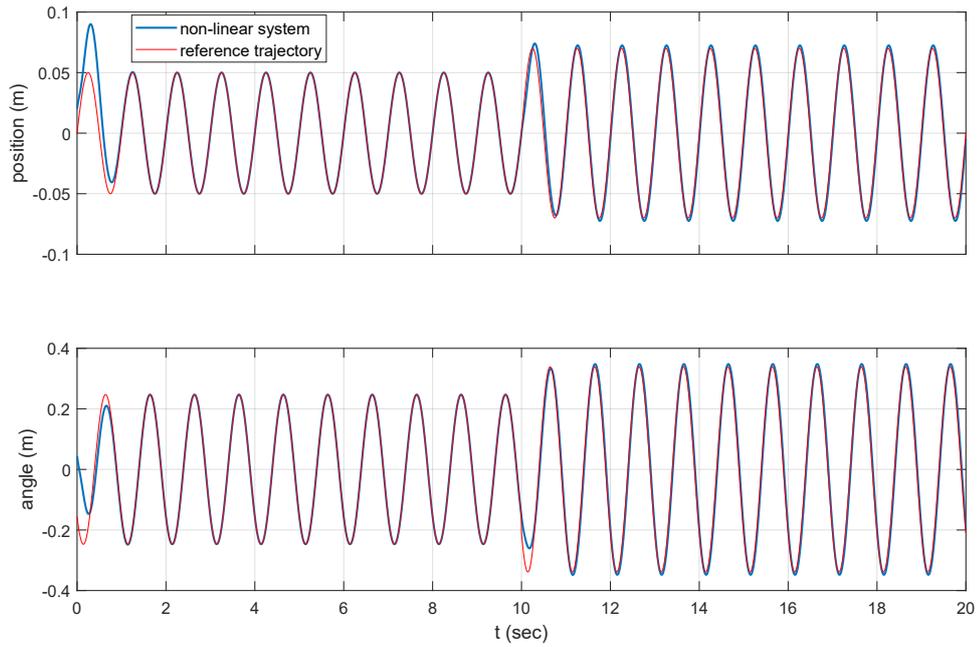
Figure 4.13: Feedback controlled step response to limit cycle amplitude change from 4.1 to 4.3 at 10 sec. with K = [81.75 6.71 19.99 7.11]
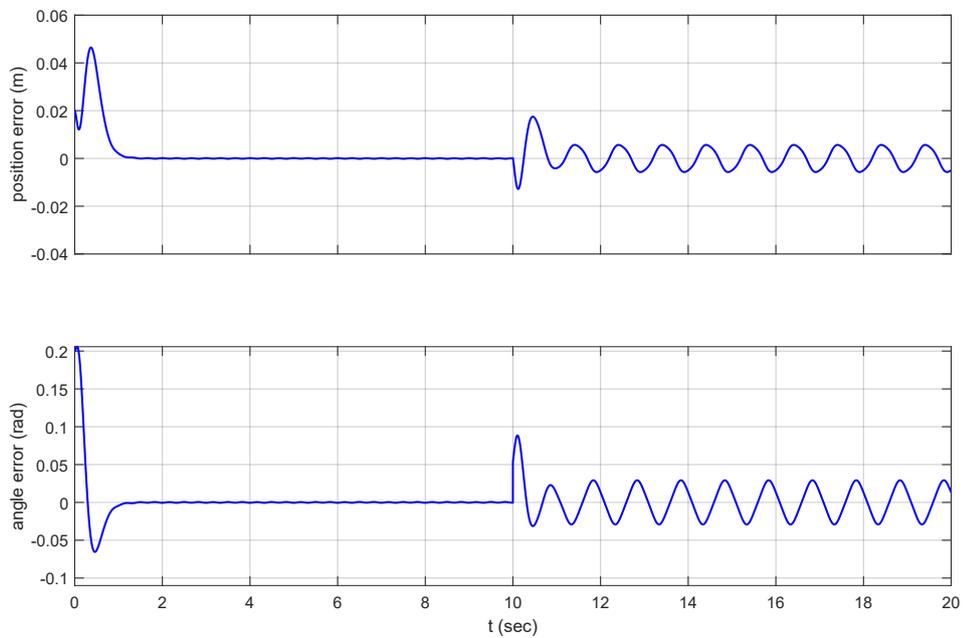
Figure 4.14: Error of the feedback controlled step response to limit cycle amplitude change from 4.1 to 4.3 at 10 sec. with K = [81.75 6.71 19.99 7.11]
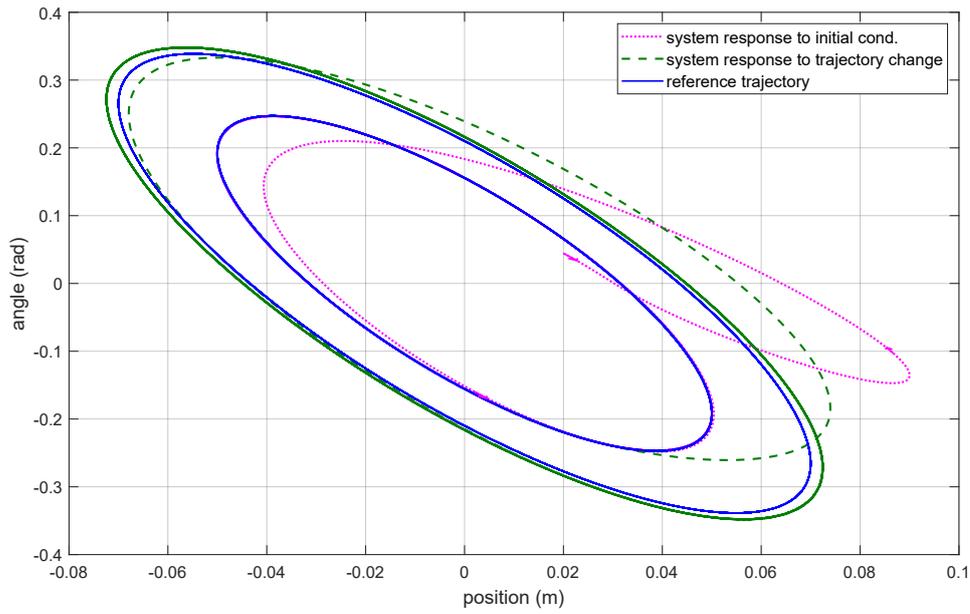
Figure 4.15: Feedback controlled trajectory for limit cycle amplitude change from 4.1 to 4.3. with K = [81.75 6.71 19.99 7.11]
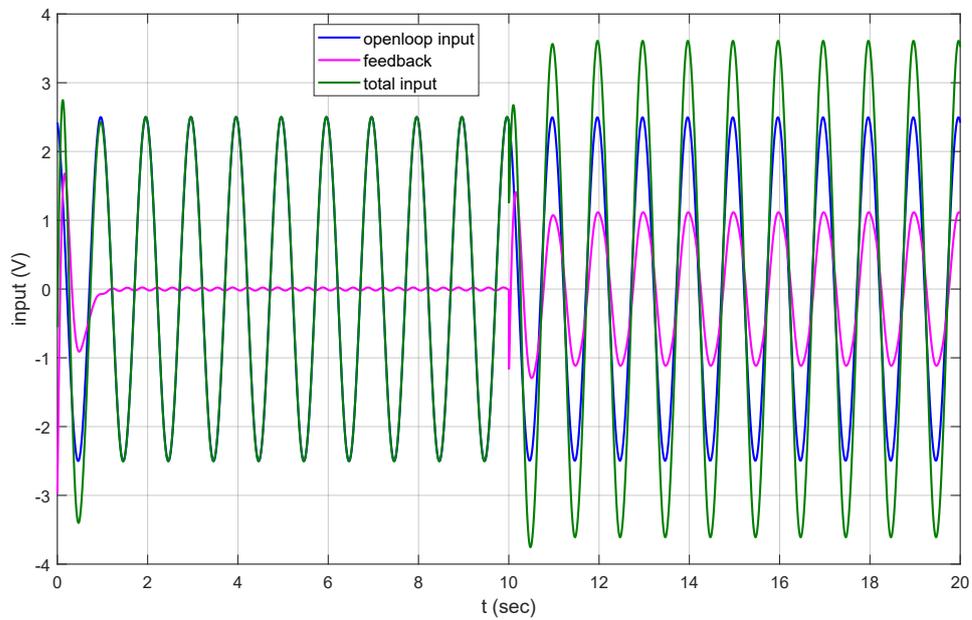
Figure 4.16: Input with reference trajectory changed from 4.1 to 4.3 at 10 sec. with K = [81.75 6.71 19.99 7.11]

4.1.5 Step Response: Limit Cycle Phase

Another scenario is to change the phase of the reference trajectory during execution. This can be considered as speeding up the system for a short amount of time. Along with the reference position and angle trajectories, open-loop input phase is also changed the same amount. In this case, the limit cycle stays the same but we want the system to jump to a phase point that is normally ahead (in time), which is equivalent to increasing the clock-rate of the oscillator. In Figures 4.17, 4.18, 4.19, 4.20, 4.21 and 4.22 we see the output of the system to phase changes of $\pi/4\ rad$, $\pi/2\ rad$ and $\pi\ rad$ on the trajectory (4.1).
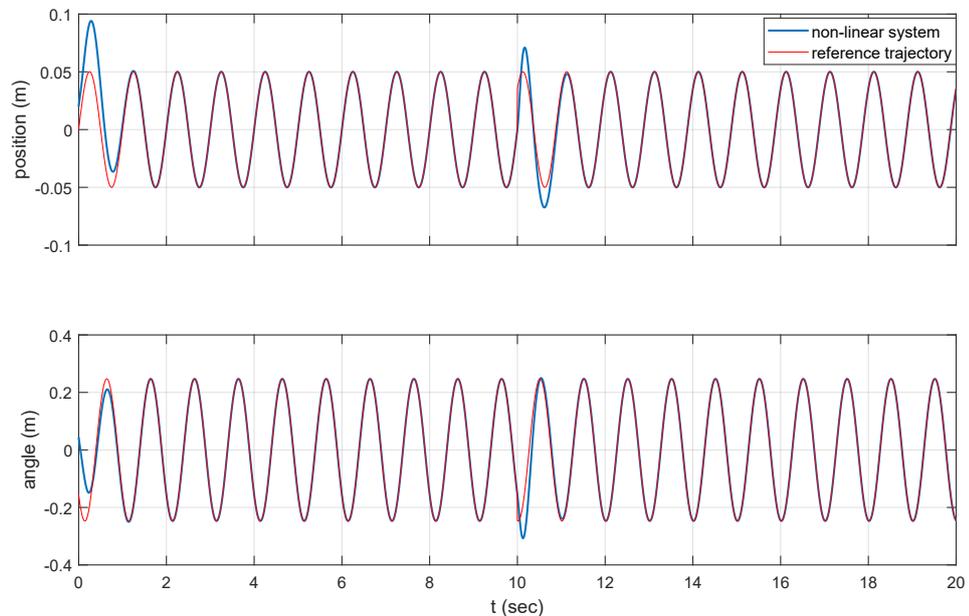
Figure 4.17: Feedback controlled system response with reference trajectory phase set forward $\pi/4\ rad$ at 10 sec. with K =[70.24 -1.93 19.79 6.6]

41
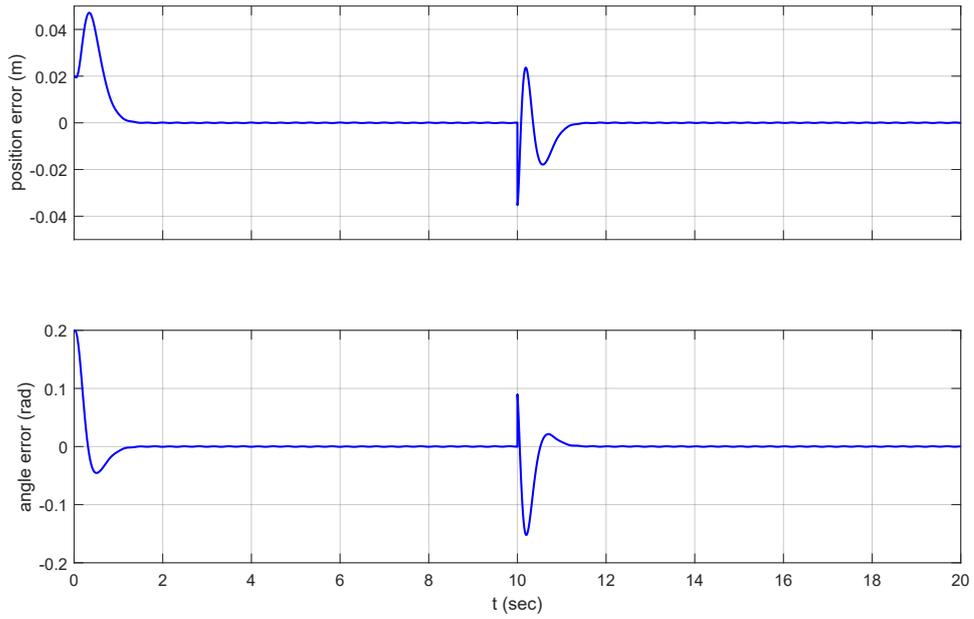
Figure 4.18: Error of the feedback controlled system response with reference trajectory phase set forward $\pi/4\ rad$ at 10 sec. with K =[70.24 -1.93 19.79 6.6]
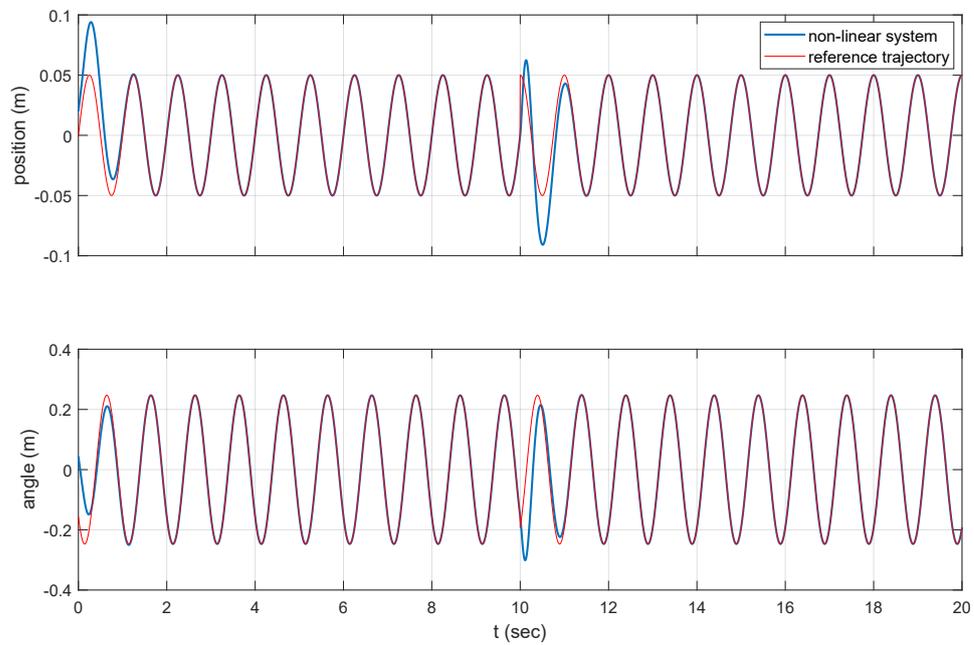
Figure 4.19: Feedback controlled system with reference trajectory phase set forward $\pi/4\ rad$ at 10 sec. with K =[70.24 -1.93 19.79 6.6]
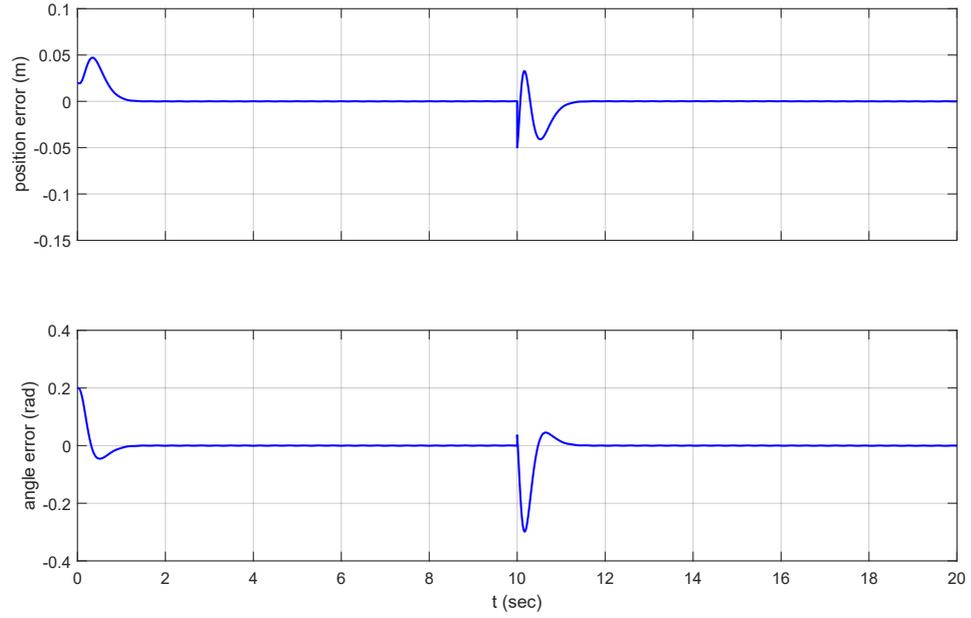
Figure 4.20: Error of the feedback controlled system response with reference trajectory phase set forward $\pi/2\ rad$ at 10 sec. with K =[70.24 -1.93 19.79 6.6]
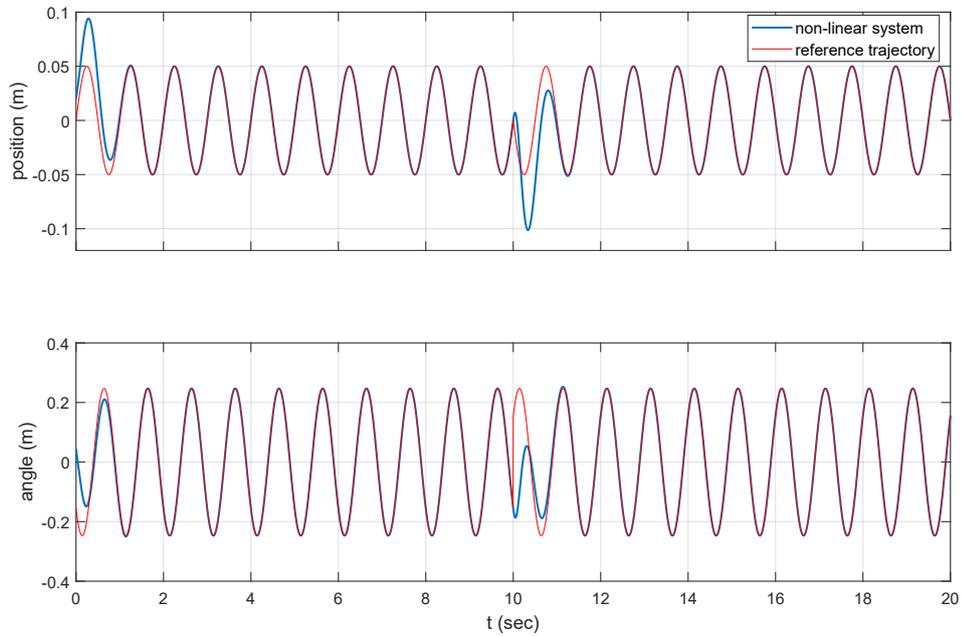
Figure 4.21: Feedback controlled system response with reference trajectory phase set forward $\pi/4\ rad$ at 10 sec. with K =[70.24 -1.93 19.79 6.6]
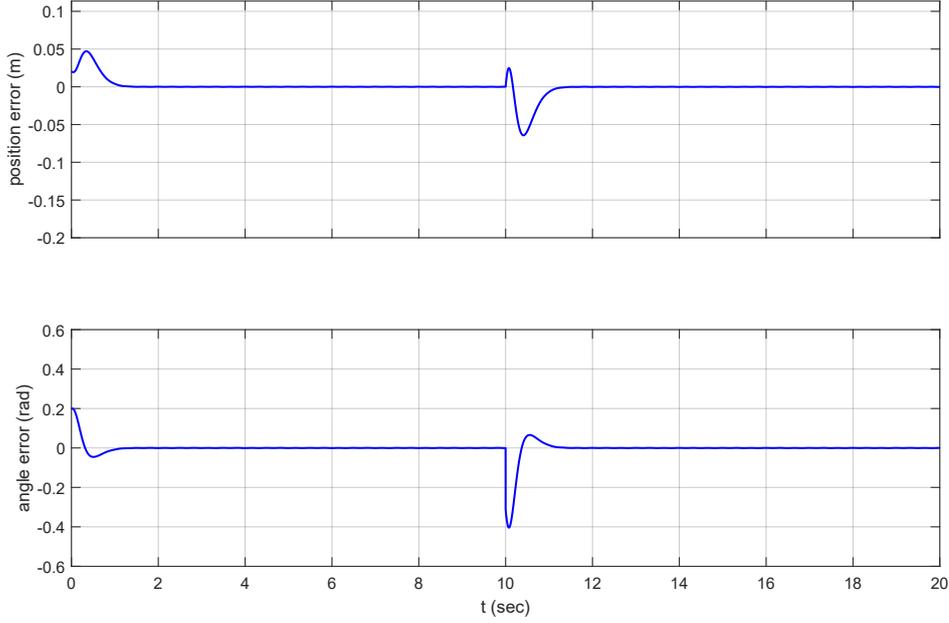
Figure 4.22: Error of the feedback controlled system response with reference trajectory phase set forward π rad at 10 sec. with K =[70.24 -1.93 19.79 6.6]

4.1.6 Comparison with Simulation Based Optimization

In order to evaluate the performance of the proposed controller design procedure, we also designed a controller by directly simulating the non-linear system. In this optimization, we solve the problem,

$$K = \underset{K \in \Re^4}{\arg \min} \left(5\sqrt{\int (x(t) - x_{ref}(t))^2 dt} + \sqrt{\int (\theta(t) - \theta_{ref}(t))^2 dt} \right) \tag{4.4}$$
$$\text{subject to}: \; ||K||_2 - 1000 < 0$$

using the particle swarm optimization algorithm 1 minimizing the weighted root mean squared error at the output of the dynamical system simulation. The purpose of the weight is to balance the errors of cart position and pendulum angle, since one is in meters and the other in radians. Constraint imposed on K ensures to keep the control input at reasonable levels. $|| \cdot ||_2$ signifies the Euclidean norm. In Figures 4.23 and 4.24 we see the output of 50 iterations of this optimization algorithm. Looking at this result, we can claim that we can design a similar (or sometimes even better) performing controller with harmonic balance approximation based design procedure with a much lower, about 10000 times less, computational effort.

44
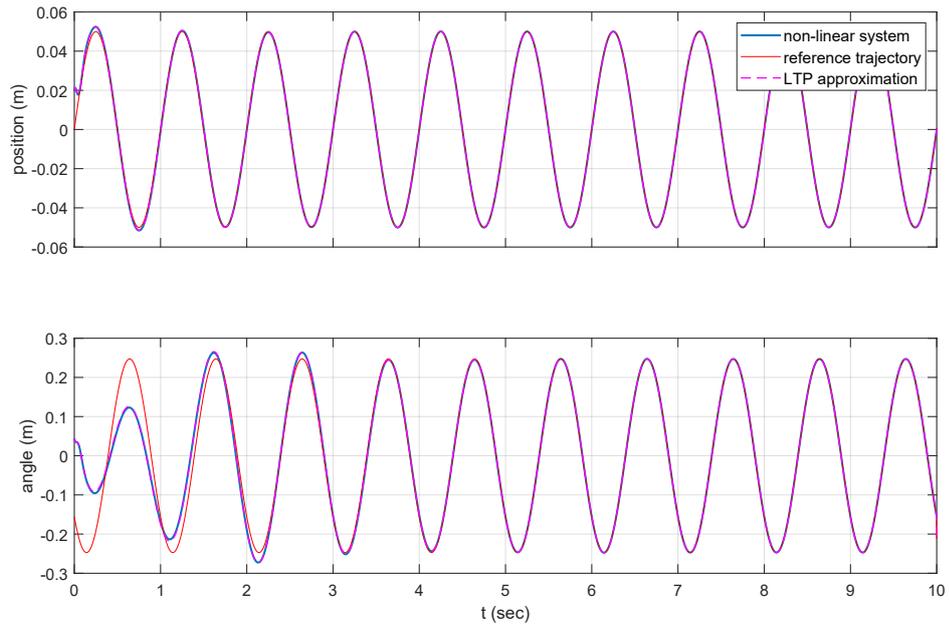
Figure 4.23: Feedback controlled system response to a feedback vector, K= [872.59 -8.88 13.6 1.2], obtained as a result of simulation based optimization
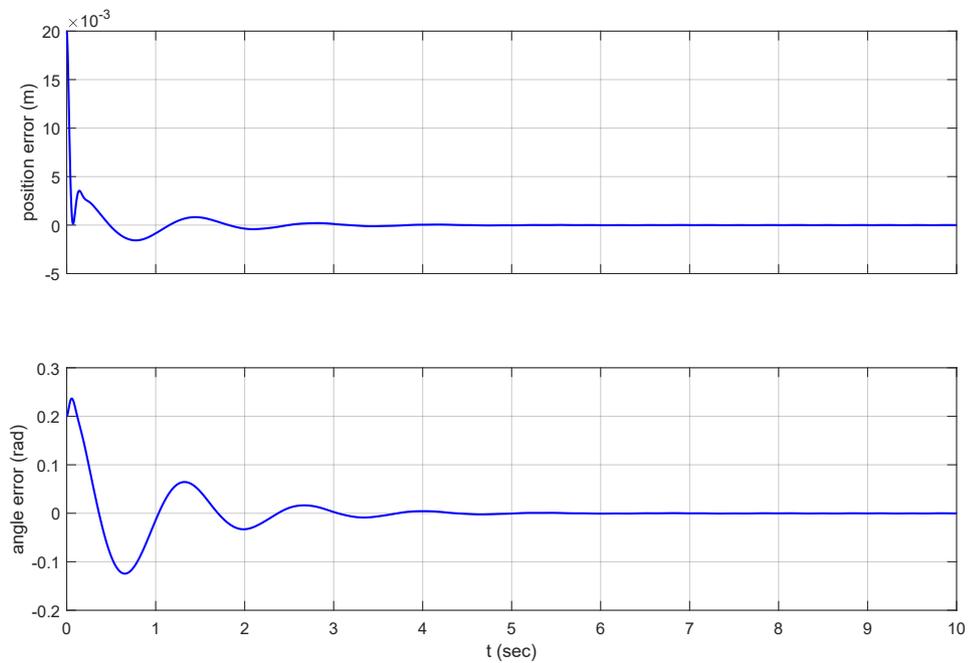
Figure 4.24: Error of the feedback controlled system response to a feedback vector, K= [872.59 -8.88 13.6 1.2], obtained as a result of simulation based optimization

45

4.1.7 Discussion

We analyzed the proposed controller design method around the stable limit cycles for the example system. We observed that for this case, linearization around periodic trajectories is valid and useful for a wide region and the system can be approximated with very small approximation error with its harmonic balance representation. So we were able to utilize an LTI controller on the basis of this lifted LTI representation of the originally nonlinear system increasing convergence rate and successfully tracking position, amplitude, and phase changes in the reference limit cycle.

4.2 Inverted Pendulum

In this section, we investigate the validity of the control procedure for unstable limit cycles around the upright equilibrium point of the cart-pendulum system. Rotational spring coefficient K_s is taken to be $0.74 \ N \cdot m/rad$ rendering the open loop limit cycles unstable on the verge of stability.

4.2.1 Open-Loop Behavior

For the system around unstable equilibrium point, eigenvalues of the approximated LTP system detailed in Table 4.2 and Figure 4.25 suggest that the LTP system is marginally stable, even tough the original nonlinear system is unstable, which can be seen from Figure 4.26. From this observation we can say that the harmonic balance approximation fails to capture the dynamics of the linearized LTP system completely or the linearized system does not represent the nonlinear system well enough.

Table 4.2: Open-loop eigenvalues of the truncated LTI approximation for a limit cycle around the unstable equilibrium with frequency $\omega_0 = 10\pi \ rad/s$

0.0000 +62.8319i	-0.2282 +62.8312i	-1.7123 +62.8325i	-19.8331 +62.8318i
0.0000 +31.4159i	-0.2282 +31.4152i	-1.7123 +31.4165i	-19.8331 +31.4159i
0.0000 + 0.0000i	-0.2295 - 0.0000i	-1.7110 + 0.0000i	-19.8332 - 0.0000i
0.0000 -31.4159i	-0.2282 -31.4152i	-1.7123 -31.4165i	-19.8331 -31.4159i
0.0000 -62.8319i	-0.2282 -62.8312i	-1.7123 -62.8325i	-19.8331 -62.8318i

Figure 4.25: Open-loop eigenvalues of the truncated LTI approximation and the LTI component of the LTP system (A_0) for a limit cycle around the unstable equilibrium with frequency $\omega_0 = 10\pi \ rad/s$
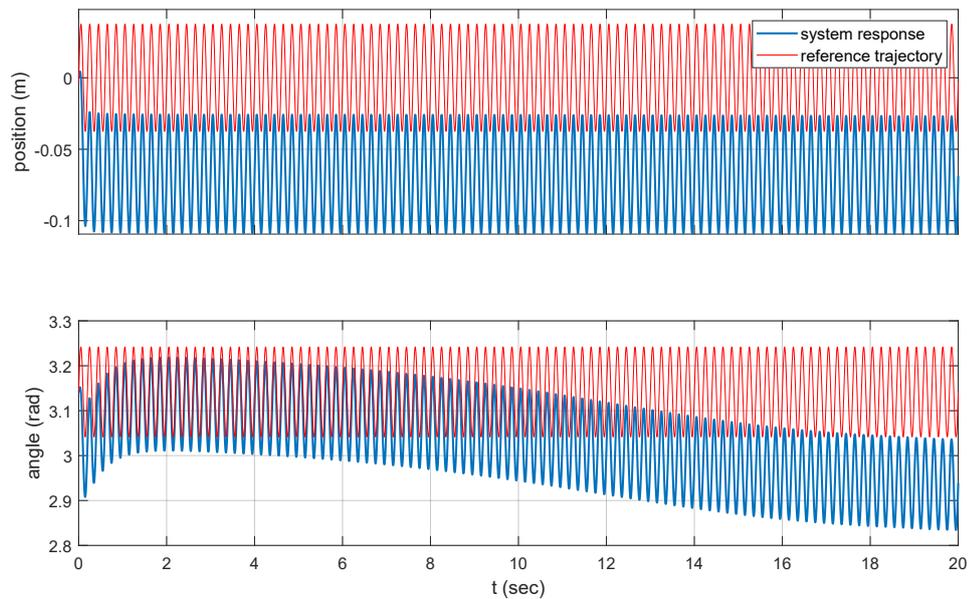
Figure 4.26: Open-loop controlled response of the original nonlinear system around an unstable limit cycle with frequency $\omega_0 = 10\pi \ rad/s$ to zero initial conditions

47

4.2.2 Closed-Loop Behavior

Even though, harmonic balance approximation may not accurately represent the open-loop unstable nonlinear system, we further investigated the closed-loop behavior with hope that feedback could reduce the uncertainties and approximation errors. Through investigation of the stabilizing feedback gain values and eigenvalue locations, we develop an optimization algorithm that outputs stabilizing controllers. Solving this optimization problem also presented in Section 3.3.3 for the trajectory,

$$\theta(t) = \pi + 0.1\sin(10\pi t)\ rad$$
$$x(t) = 3.75 \times 10^{-2}\sin(10\pi t - 0.0769)\ m \quad\quad (4.5)$$
$$V(t) = 14.0857\sin(10\pi t + 2.6703)V$$

we obtained different solutions due to the randomness inherent in the PSO optimization algorithm. However, the system response were generally similar to each other. One example result is illustrated in Figures 4.27, 4.28, 4.29, and 4.30 There is about a maximum of 10% error in angle, and a maximum of 9.21% error in position in steady-state conditions.
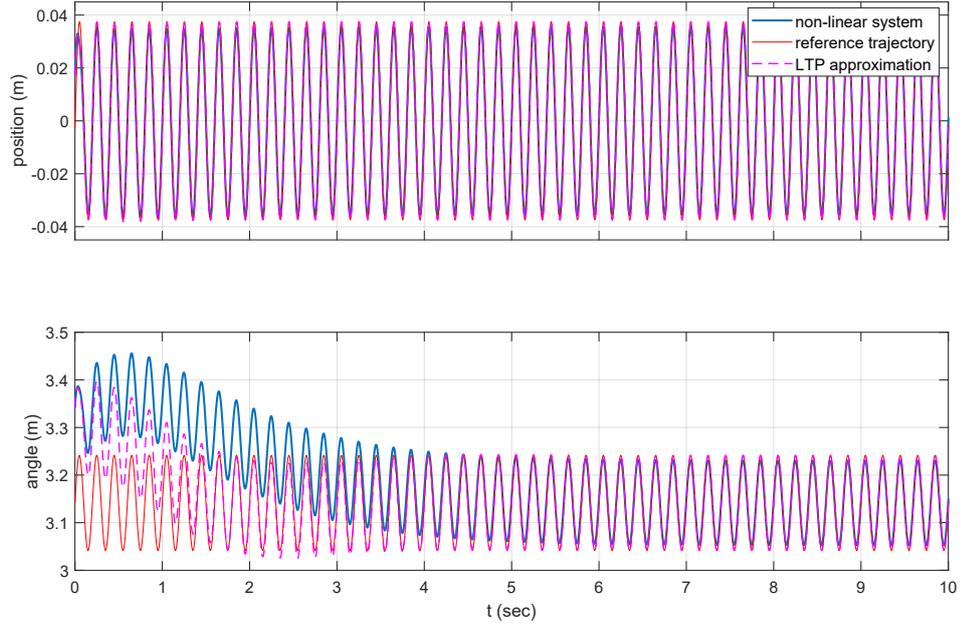
Figure 4.27: Feedback controlled system response around the unstable limit cycle 4.5 with frequency $\omega_0 = 10\pi\ rad/s$ with initial conditions $[x\ \theta\ \dot{x}\ \dot{\theta}] = [0.01\ m\ 0.05\ rad\ 0\ 0]$ deviating from the limit cycle and $\mathbf{K}=10^3[1.0005\ 0.0039\ 0.0054\ -0.0007]$
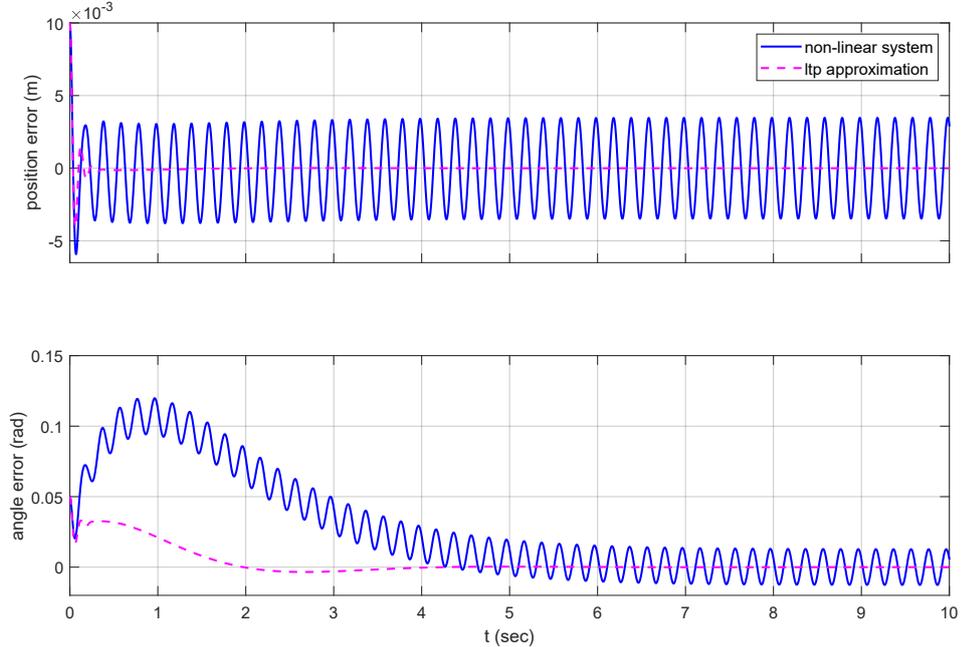
Figure 4.28: Error of the feedback controlled system response around the unstable limit cycle 4.5 with frequency $\omega_0 = 10\pi\ rad/s$ with initial conditions $[x\ \theta\ \dot{x}\ \dot{\theta}] = [0.01\ m\ 0.05\ rad\ 0\ 0]$ deviating from the limit cycle and $\mathbf{K}=10^3[1.0005\ 0.0039\ 0.0054\ -0.0007]$
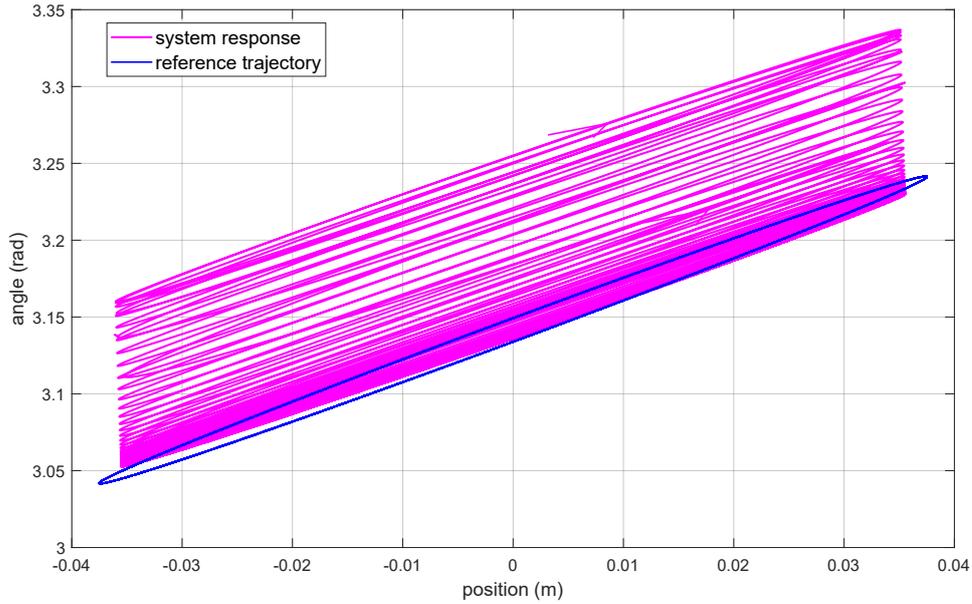
Figure 4.29: Feedback controlled trajectory around the unstable limit cycle 4.5 with frequency $\omega_0 = 10\pi \ rad/s$ with initial conditions $[x \ \theta \ \dot{x} \ \dot{\theta}] = [0.01 \ m \ 0.05 \ rad \ 0 \ 0]$ deviating from the limit cycle and K=$10^3[1.0005 \ 0.0039 \ 0.0054 \ -0.0007]$

Unlike the stable limit-cycle eigenvalues inside the primary strip of the closed-loop system in harmonic balance form and the eigenvalues of the $A_0 - B_0K$ component are very close to each other as can be seen from figure 4.30. This implies that the closed-loop system is almost in Floquet form even after feedback which is a quite surprising result.
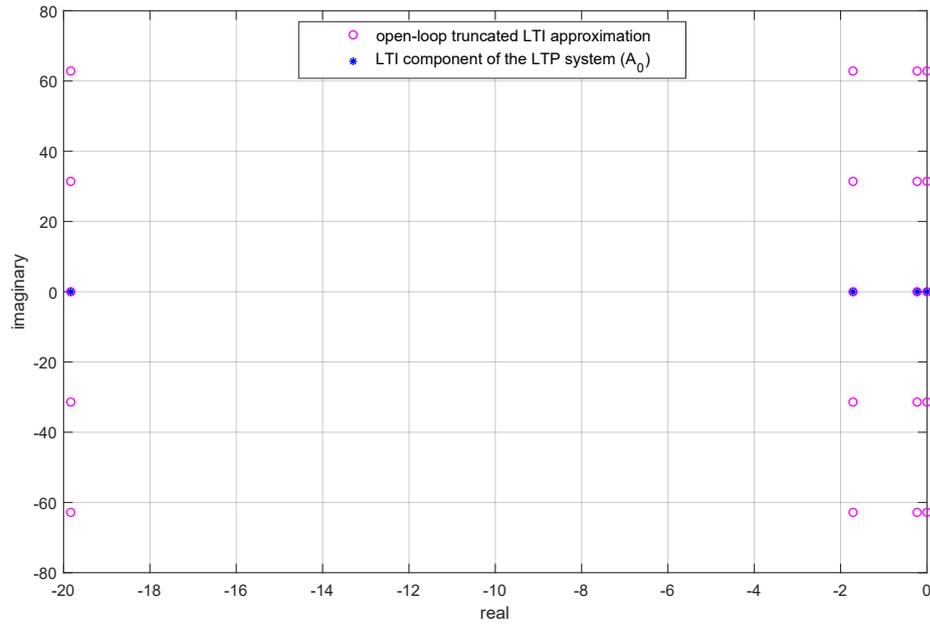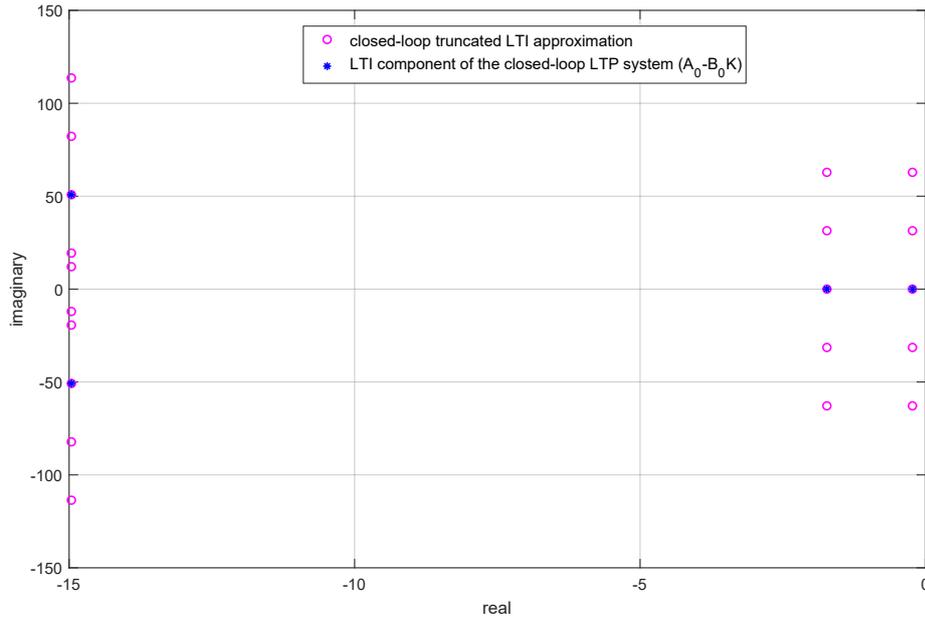
Figure 4.30: Closed-loop eigenvalues of the truncated LTI approximation and the LTI component of the closed-loop LTP system $(A_0 - B_0 K)$ for a limit cycle around the unstable equilibrium point with frequency $\omega_0 = 10\pi \ rad/s$ and K = $10^3[1.0005 \ 0.0039 \ 0.0054 \ - 0.0007]$

4.2.3 Failing Cases

We have observed in the open-loop that there is some inconsistency between the responses of nonlinear and linearized systems. We investigated in what conditions this inconsistency occurred to develop a working controller design method starting with the one we developed for the stable limit cycles.

Figure 4.31 exemplifies a case when the LTP approximation does not accurately represents the behavior of the nonlinear system. As can be seen from Table 4.3 that the eigenvalues of the LTI representation indicate that the system should be stable and LTP approximation follows this behavior. To recover from this problem, a different linearization procedure can be adopted to better approximate the nonlinear system. However, this is left as a future work.
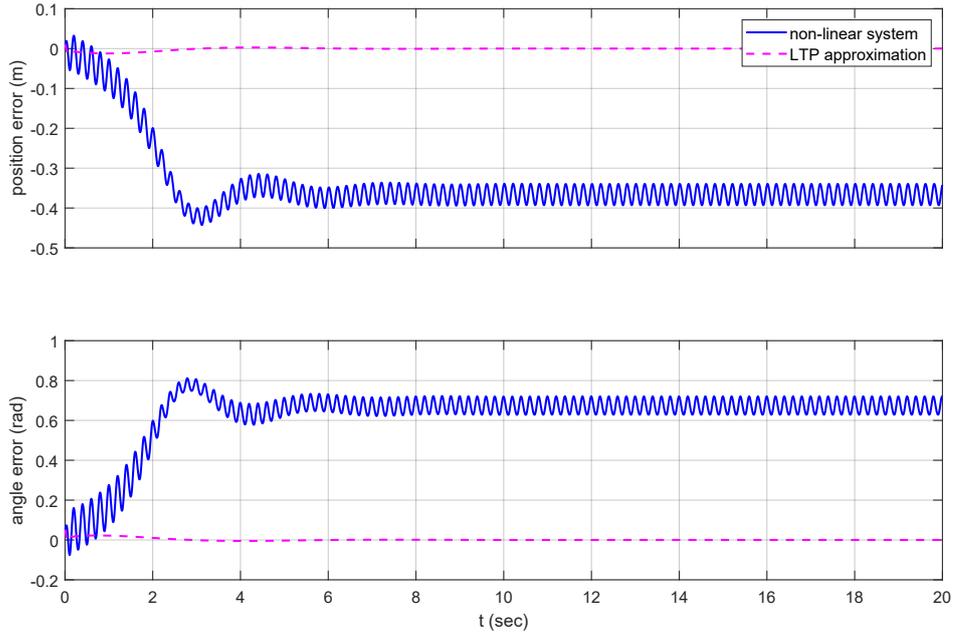
Figure 4.31: Error of the feedback controlled system around an unstable limit cycle with K=[397.1490 216.1851 47.4926 -17.5772] making the original nonlinear system unstable while rendering the LTI approximation eigenvalues with negative real parts and the LTP approximation stable

Table 4.3: Closed-loop eigenvalues of the truncated LTI approximation for a limit cycle around the unstable equilibrium with frequency $\omega_0 = 10\pi \ rad/s$ and K= [397.1490 216.1851 47.4926 -17.5772] making the nonlinear system unstable

-00.39 + 62.75i	-00.39 + 62.91i	-15.56 + 11.63i	-15.56 + 114.04i
-00.39 + 31.33i	-00.39 + 31.50i	-15.56 - 19.79i	-15.56 + 82.62i
-00.39 - 00.11i	-00.39 + 00.11i	-15.56 - 51.21i	-15.56 + 51.21i
-00.39 - 31.50i	-00.39 - 31.33i	-15.56 - 82.62i	-15.56 + 19.79i
-00.39 - 62.91i	-00.39 - 62.75i	-15.56 - 114.04i	-15.56 - 11.63i

Another example of the mismatching cases can be seen in figure 4.32. Here both the nonlinear and the LTP systems exhibit unstable behavior even though the eigenvalues of the LTI system are in the stable region. LTP system being unstable in this case indicates that the order of truncation should be higher which is also left for future work.
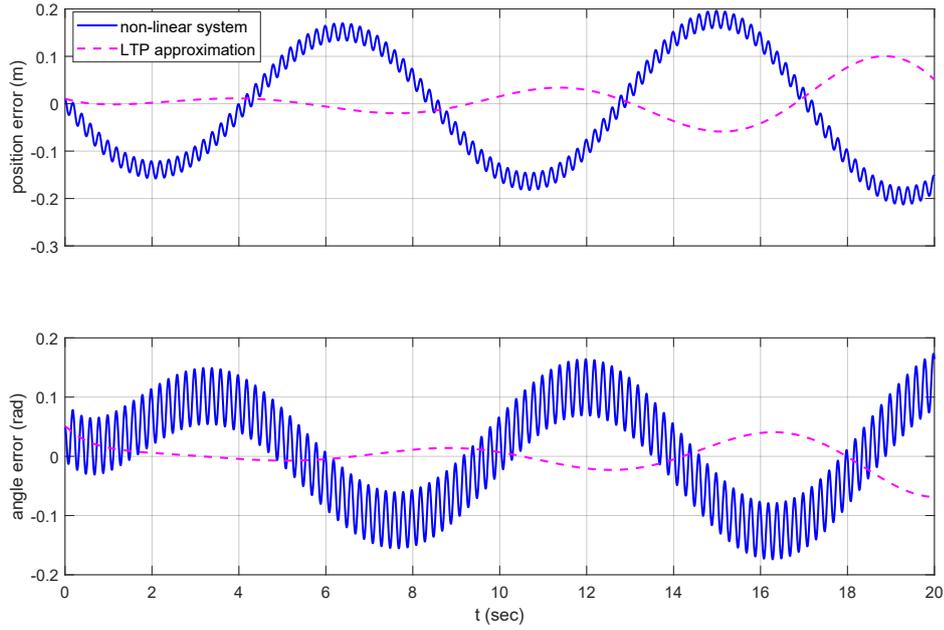
Figure 4.32: Error of the feedback controlled system around an unstable limit cycle with K=[4.3564 4.9899 -8.8605 4.8718] making the original nonlinear system and the LTP approximation unstable while rendering the LTI approximation eigenvalues with negative real parts

Table 4.4: Closed-loop eigenvalues for a limit cycle around the unstable equilibrium with K= [4.3564 4.9899 -8.8605 4.8718] making both the nonlinear system and the LTP system unstable

-0.4039 +62.8254i	-0.4056 +62.3460i	-0.4041 +63.3240i	-29.6538 +62.8319i
-0.4039 +31.4094i	-0.4056 +30.9301i	-0.4041 +31.9081i	-29.6538 +31.4160i
-0.4058 - 0.0000i	-0.4039 - 0.4888i	-0.4039 + 0.4888i	-29.6538 - 0.0000i
-0.4039 -31.4094i	-0.4041 -31.9081i	-0.4056 -30.9301i	-29.6538 -31.4160i
-0.4039 -62.8254i	-0.4041 -63.3240i	-0.4056 -62.3460i	-29.6538 -62.8319i

4.2.4 Comparison with Simulation Based Optimization

For the unstable limit cycles unlike the stable limit cycle case we use the resulting feedback gain and eigenvalue places of the simulation based optimization to understand system behavior and to impose better constraints on the eigenvalue optimization procedure. Using the particle swarm optimization algorithm 1 we solve the following

optimization problem

$$K = \underset{K \in \Re^4}{\arg\min} \left(\sqrt{\int (x(t) - x_{ref}(t))^2 dt} + \sqrt{\int (\theta(t) - \theta_{ref}(t))^2 dt} \right.$$

$$\left. + 10 \left(\sqrt{\int (x_{ss}(t) - x_{ref}(t))^2 dt} + \sqrt{\int (\theta_{ss}(t) - \theta_{ref}(t))^2 dt} \right) \right) \quad (4.6)$$

$$\text{subject to}: \ ||K||_2 - 1500 < 0.$$

Since there is steady state error for this case, the objective function is defined as the weighted summation of the root mean squared error and the root mean squared error in steady state condition in order to minimize both the steady state error and the settling time. Figures 4.33 and 4.34 illustrate the output of 30 iterations of this optimization procedure. We observe that in this case we obtain a similar settling time performance with the eigenvalue optimization based controller and a better steady state performance with a maximum of 4.56 % and a maximum of 8.3 % error for cart position and pendulum angle, which are 4.65 % and 1.7 % less compared to the eigenvalue optimization based controller. The difference between the steady state errors are not significant but computation time is significantly decreased, about a 1000 times, with the eigenvalue optimization.
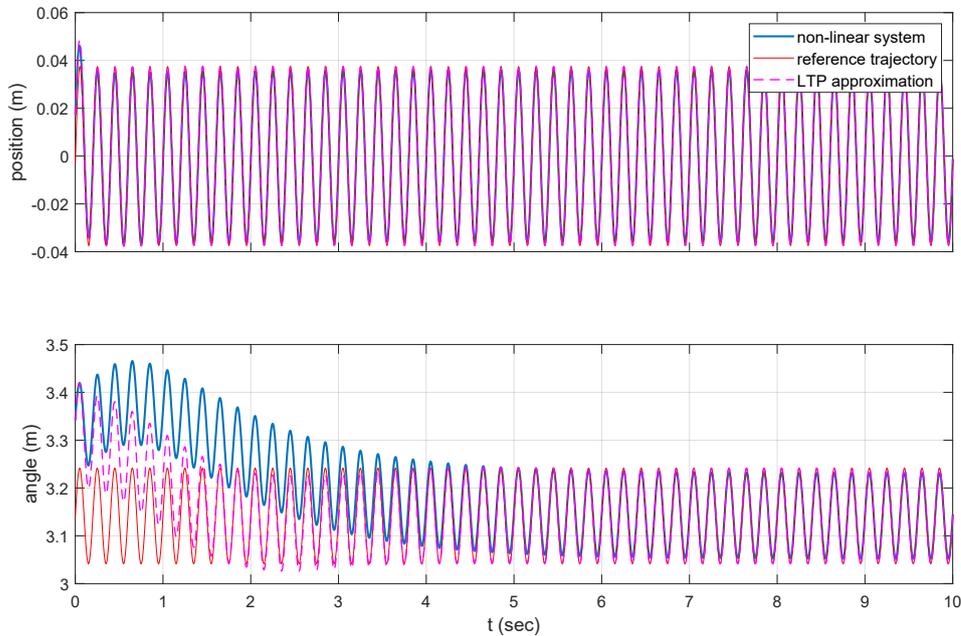
Figure 4.33: Feedback controlled system response to a feedback vector, K= 10^3[1.0932 0.0043 0.0756 0.0025], obtained as a result of simulation based optimization
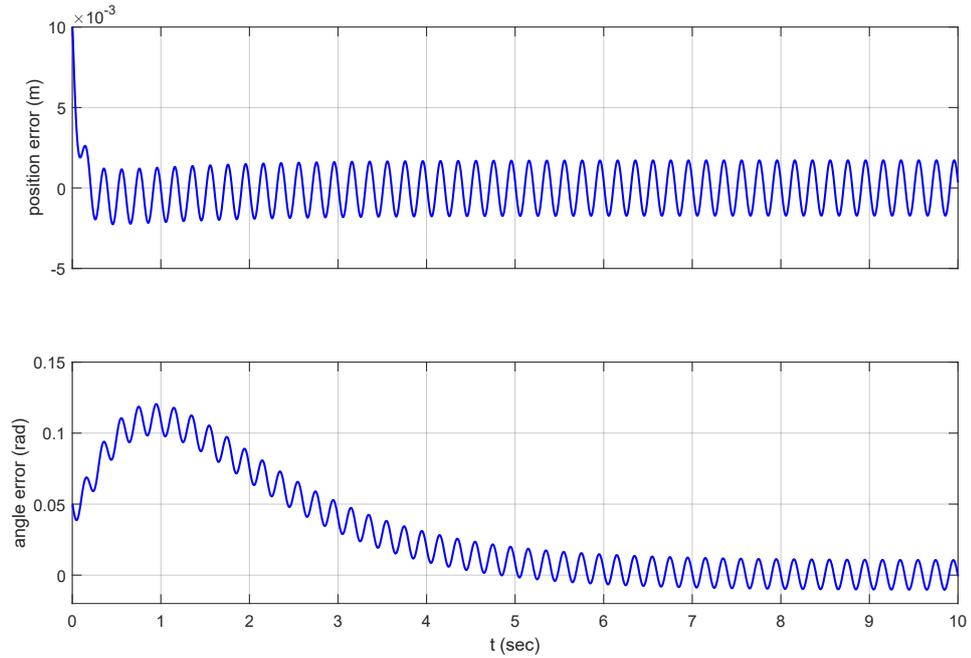
Figure 4.34: Error of the feedback controlled system response to a feedback vector, K= 10^3[1.0932 0.0043 0.0756 0.0025], obtained as a result of simulation based optimization

Table 4.5: Closed-loop eigenvalues for a limit cycle around the unstable equilibrium with K= 10^3[1.0932 0.0043 0.0756 0.0025]

-0.23 +62.83i	-1.76 +62.83i	-12.94 +62.83i	-233.14 +62.83i
-0.23 +31.42i	-1.76 +31.42i	-12.94 +31.42i	-233.14 +31.42i
-0.23 + 0.00i	-1.76 - 0.00i	-12.94 + 0.00i	-233.14 - 0.00i
-0.23 -31.42i	-1.76 -31.42i	-12.94 -31.42i	-233.14 -31.42i
-0.23 -62.83i	-1.76 -62.83i	-12.94 -62.83i	-233.14 -62.83i

4.2.5 Discussion

We applied the controller design procedure developed for stable limit cycles to stabilize the system around unstable limit cycles and observed that a direct adaptation was not valid. We observed that the linearization procedure did not capture the original nonlinear system dynamics completely and the LTI approximation did not represent the LTP system accurately for every feedback coefficient. However, by analyzing the system response under different conditions we were able to develop a design procedure that works around the mismatches caused by linearization and left recovering

55

for them as future work.

CHAPTER 5

CONCLUSION

Analysis and control of periodic trajectories in underactuated nonlinear systems posses great importance in robotics, especially in legged locomotion. Control of these trajectories is a relatively new concern and the few methods existent in the literature mostly result in time-dependent controllers. We propose a controller design method that generates time invariant state feedback controllers that can stabilize underactuated nonlinear systems around their periodic trajectories. We applied our method on the widely used cart-pendulum example for periodic trajectories around the both stable and unstable equilibrium points.

Stable limit cycles respond to the proposed method quite well. We observed that linearization both in LTP form and in LTI form represents the nonlinear system very accurately and the control strategy is valid for a wide region around the limit cycle. We were able to enhance convergence performance and track position, amplitude and phase changes in the limit cycle. However, for unstable orbits there is a mismatch between the responses of linearized systems (in LTP or LTI form) and the nonlinear system. We tried to overcome this issue by adapting our controller design method to the circumstances and were able to obtain a stabilizing controller using the linearized system eigenvalues. We leave developing a more reliable and provable controller design method as future work. There are several possible ways of achieving this. Adding a partial feedback linearization in the loop might increase the validity of the trajectory linearization. Another possible way is to employ transverse linearization which may result in a better LTP approximation. One other consideration as future work is to analyze the effect of truncation. By increasing the order of truncation we

may be able to obtain better performance for especially the unstable orbits. Another improvement can be in the computational process. For the example system examined here, only the even numbered Fourier coefficients are effective in the system matrices. So the LTP system pumping frequency is twice the frequency of the linearization orbit which results in sparse Toeplitz matrices. Getting rid of zero elements in these matrices may allow us to take more harmonics into account without losing computational power. One final idea as a future work is including the imaginary parts of the LTI system's eigenvalues to the objective function in order to control the overshoot performance.

REFERENCES

[1] A. D. Ames, K. Galloway, K. Sreenath, and J. W. Grizzle, "Rapidly exponentially stabilizing control lyapunov functions and hybrid zero dynamics," *IEEE Transactions on Automatic Control*, vol. 59, no. 4, pp. 876–891, 2014.

[2] A. D. Ames, "Human-inspired control of bipedal walking robots.," *IEEE Trans. Automat. Contr.*, vol. 59, no. 5, pp. 1115–1130, 2014.

[3] K. A. Hamed, B. G. Buss, and J. W. Grizzle, "Exponentially stabilizing continuous-time controllers for periodic orbits of hybrid systems: Application to bipedal locomotion with ground height variations," *The International Journal of Robotics Research*, vol. 35, no. 8, pp. 977–999, 2016.

[4] H. Dai and R. Tedrake, "Optimizing robust limit cycles for legged locomotion on unknown terrain," in *Decision and Control (CDC), 2012 IEEE 51st Annual Conference on*, pp. 1207–1213, Citeseer, 2012.

[5] E. R. Westervelt, J. W. Grizzle, and D. E. Koditschek, "Hybrid zero dynamics of planar biped walkers," *IEEE Transactions on Automatic Control*, vol. 48, pp. 42–56, Jan 2003.

[6] M. M. Ankarali and U. Saranli, "Stride-to-stride energy regulation for robust self-stability of a torque-actuated dissipative spring-mass hopper," *Chaos*, vol. 20, Sep. 2010.

[7] M. M. Ankarali, S. Sefati, M. S. Madhav, A. Long, A. Bastian, and N. J. Cowan, "Walking dynamics are symmetric (enough)," vol. 12, no. 108, p. 20150209, 2015.

[8] M. M. Ankarali and N. J. Cowan, "System identification of rhythmic hybrid dynamical systems via discrete time harmonic transfer functions," (Los Angeles, CA, USA), December 2014.

[9] I. Uyanik, M. M. Ankarali, N. J. Cowan, O. Morgul, and U. Saranli, "Toward data-driven models of legged locomotion using harmonic transfer functions," (Istanbul, Turkey), pp. 357–362, IEEE, July 2015.

[10] E. D. Tytell, J. A. Carr, N. Danos, C. Wagenbach, C. M. Sullivan, T. Kiemel, N. J. Cowan, and M. M. Ankarali, "Body stiffness and damping depend sensitively on the timing of muscle activation in lampreys," 2018.

[11] M. S. Allen, M. W. Sracic, S. Chauhan, and M. H. Hansen, "Output-only modal analysis of linear time-periodic systems with application to wind turbine simulation data," *Mechanical Systems and Signal Processing*, vol. 25, no. 4, pp. 1174 – 1191, 2011.

[12] C. L. Bottasso and S. Cacciola, "Model-independent periodic stability analysis of wind turbines," *Wind Energy*, vol. 18, no. 5, pp. 865–887, 2015.

[13] P. Arcara, S. Bittanti, and M. Lovera, "Periodic control of helicopter rotors for attenuation of vibrations in forward flight," *IEEE Transactions on Control Systems Technology*, vol. 8, pp. 883–894, Nov 2000.

[14] S. Hwang, *Frequency domain system identification of helicopter rotor dynamics incorporating models with time periodic coefficients*. PhD thesis, University of Maryland, College Park, August 1997.

[15] E. Möllerstedt, *Dynamic analysis of harmonics in electrical systems*. PhD thesis, Department of Automatic Control, Lund Institute of Technology, 2000.

[16] E. Möllerstedt and B. Bernhardsson, "A harmonic transfer function model for a diode converter train," in *2000 IEEE Power Engineering Society Winter Meeting. Conference Proceedings (Cat. No.00CH37077)*, vol. 2, pp. 957–962 vol.2, Jan 2000.

[17] J. Kwon, X. Wang, F. Blaabjerg, and C. L. Bak, "Frequency-domain modeling and simulation of dc power electronic systems using harmonic state space method," *IEEE Transactions on Power Electronics*, vol. 32, pp. 1044–1055, Feb 2017.

[18] J. R. C. Orillaza and A. R. Wood, "Harmonic state-space model of a controlled tcr," *IEEE Transactions on Power Delivery*, vol. 28, pp. 197–205, Jan 2013.

[19] L. Freidovich, A. Robertsson, A. Shiriaev, and R. Johansson, "Periodic motions of the pendubot via virtual holonomic constraints: Theory and experiments," *Automatica*, vol. 44, no. 3, pp. 785 – 791, 2008.

[20] L. B. Freidovich, A. S. Shiriaev, and I. R. Manchester, "Stability analysis and control design for an underactuated walking robot via computation of a transverse linearization," *IFAC Proceedings Volumes*, vol. 41, no. 2, pp. 10166 – 10171, 2008. 17th IFAC World Congress.

[21] M. Maggiore and L. Consolini, "Virtual holonomic constraints for euler–lagrange systems," *IEEE Transactions on Automatic Control*, vol. 58, pp. 1001–1008, April 2013.

[22] A. Shiriaev, L. Freidovich, and I. Manchester, "Can we make a robot ballerina perform a pirouette? orbital stabilization of periodic motions of underactuated

mechanical systems," *Annual Reviews in Control*, vol. 32, no. 2, pp. 200 – 211, 2008.

[23] A. S. Shiriaev, L. B. Freidovich, and S. V. Gusev, "Transverse linearization for controlled mechanical systems with several passive degrees of freedom," *IEEE Transactions on Automatic Control*, vol. 55, pp. 893–906, April 2010.

[24] A. Shiriaev, J. W. Perram, and C. C. de Wit, "Constructive tool for orbital stabilization of underactuated nonlinear systems: virtual constraints approach," *IEEE Transactions on Automatic Control*, vol. 50, pp. 1164–1176, Aug 2005.

[25] Z. Wang, L. B. Freidovich, and H. Zhang, "Periodic motion planning and control for double rotary pendulum via virtual holonomic constraints," *IEEE/CAA Journal of Automatica Sinica*, pp. 1–8, 2018.

[26] L. Freidovich, A. Shiriaev, F. Gordillo, F. Gomez-Estern, and J. Aracil, "Partial-energy-shaping control for orbital stabilization of high frequency oscillations of the furuta pendulum," in *2007 46th IEEE Conference on Decision and Control*, pp. 4637–4642, Dec 2007.

[27] G. Floquet, "Sur les equations differentielles lineaires," *Ann. ENS [2]*, vol. 12, no. 1883, pp. 47–88, 1883.

[28] S. Bittanti and P. Bolzern, "Stabilizability and detectability of linear periodic systems," *Systems & control letters*, vol. 6, no. 2, pp. 141–145, 1985.

[29] J. Hauser and C. C. Chung, "Converse lyapunov functions for exponentially stable periodic orbits," in *Decision and Control, 1993., Proceedings of the 32nd IEEE Conference on*, pp. 3195–3199, IEEE, 1993.

[30] F. Mazenc, "Strict lyapunov functions for time-varying systems," *Automatica*, vol. 39, no. 2, pp. 349–353, 2003.

[31] G. W. Hill, "On the part of the motion of the lunar perigee which is a function of the mean motions of the sun and moon," *Acta mathematica*, vol. 8, no. 1, pp. 1–36, 1886.

[32] N. M. Wereley, *Analysis and control of linear periodically time varying systems*. PhD thesis, Massachusetts Institute of Technology, 1990.

[33] S. R. Hall and N. M. Wereley, "Generalized nyquist stability criterion for linear time periodic systems," in *American Control Conference, 1990*, pp. 1518–1525, IEEE, 1990.

[34] E. K. Hidir, I. Uyanik, and Ö. Morgül, "Harmonic transfer functions based controllers for linear time-periodic systems," *Transactions of the Institute of Measurement and Control*, p. 0142331218778748, 2018.

[35] G. Da Prato and A. Ichikawa, "Quadratic control for linear periodic systems," *Applied Mathematics and Optimization*, vol. 18, pp. 39–66, Jul 1988.

[36] I. Uyanik, M. M. Ankarali, N. J. Cowan, U. Saranli, O. Morgul, and H. Ozbay, "Independent estimation of input and measurement delays for a hybrid vertical spring-mass-damper via harmonic transfer functions," in *IFAC Workshop on Time Delay Systems*, (Ann Arbor, MI, USA), June 2015.

[37] I. Uyanik, U. Saranli, Ö. Morgül, and M. M. Ankarali, "Parametric identification of hybrid linear-time-periodic systems," *IFAC Symposium on System Structures and Control*, vol. 49, no. 9, pp. 7–12, 2016.

[38] I. Uyanık, M. M. Ankaralı, N. J. Cowan, U. Saranlı, and Ö. Morgül, "Identification of a vertical hopping robot model via harmonic transfer functions," *Transactions of the Institute of Measurement and Control*, vol. 38, no. 5, pp. 501–511, 2016.

[39] I. Uyanik, U. Saranli, M. M. Ankarali, N. J. Cowan, and O. Morgul, "Frequency-domain subspace identification of linear time periodic (ltp) systems," *IEEE Transactions on Automatic Control*, 2018.

[40] H. Sandberg, E. Möllerstedt, *et al.*, "Frequency-domain analysis of linear time-periodic systems," *IEEE Transactions on Automatic Control*, vol. 50, no. 12, pp. 1971–1983, 2005.